

Decaying vacuum energy, matter creation and cosmic acceleration

Lokesh Chander* and C P Singh†

*Department of Applied Mathematics,
Delhi Technological University, Delhi-110042, India*

(Dated: April 15, 2025)

In this paper, we discuss an interacting decaying vacuum energy and dark matter empowered by gravitationally induced matter creation model, and its impact on structure formation by analysing the growth rate perturbations. Our work is motivated by the possibility that the decaying vacuum is due to quantum field theory and dark matter originates from gravitationally induced matter creation. We delve deeper into our investigation and explore both theoretical and statistical analysis of the cosmological model to test its ability to describe the evolution of the Universe. To achieve this, we use three distinct combinations of datasets from Cosmic Chronometers, Pantheon Type Ia supernovae sample, Baryon acoustic oscillations, Cosmic Microwave Background distance priors and $f(z)\sigma_8(z)$ datapoints to constrain the model parameters. Our statistical analysis employs Markov Chain Monte Carlo (MCMC) methods. The deceleration parameter shows that the model transitions from a decelerated phase to an accelerated phase of expansion. The current Hubble parameter values are estimated to be $H_0 = 67.517 \pm 0.869$ km/s/Mpc, $H_0 = 67.534 \pm 0.874$ km/s/Mpc, and $H_0 = 67.533 \pm 0.884$ km/s/Mpc using DS1, DS2 and DS3 datasets, respectively. These values of H_0 are very close to those derived from the Planck data. The effective equation of state parameter indicates an accelerating phase, with density parameter for vacuum energy exhibiting expected values. The present value of the jerk parameter deviates slightly from the Λ CDM model. However, it approaches the standard model in late time. We analyse the stability characteristics through the selection information criteria. We also perform thermodynamic analysis by studying the evolution of entropy in the Universe for the model and find it to be in agreement with the generalised second law of thermodynamics. These findings support that the proposed model effectively describes the evolutionary features of the Universe at both theoretical and observational levels.

I. INTRODUCTION

The first observational evidence for the accelerated expansion of the Universe was confirmed through Type Ia supernovae (SNIa), rightly called ‘standard candles’, as these astronomical objects have an intrinsic luminosity [1, 2]. This discovery significantly changed our understanding about the Universe and caused a resurgence in modern cosmology. Subsequent datasets: Baryon Acoustic Oscillations (BAO) [3], the Hubble parameter measurements $H(z)$ [4], and Cosmic Microwave Background (CMB) anisotropies [5] have further validated this phenomenon. According to ‘General Relativity’ (GR), this accelerated expansion is driven by a new energy density with negative pressure, referred to as ‘dark energy’ (DE), which makes up around 70% of the Universe’s total energy density. Accompanying this is ‘dark matter’ (DM), whose nature is not completely understood and together, both dark components make up for 95% of the Universe’s content [6]. Understanding the origin of DE remains one of the major unsolved issues in modern cosmology as its exact nature is still unknown. The naturally arising candidate for dark energy within the framework of GR is the cosmological constant, denoted by Λ , or equivalently, the vacuum energy density associated with it, $\rho_\Lambda = \Lambda/8\pi G$ [7]. It has a negative pressure, making it the repulsive

driving force that causes accelerated expansion under the condition that Λ has a value greater than zero [8].

However, the Λ -based concordance model faces theoretical challenges, most notably the cosmological constant problem and cosmic coincidence [9–13], which remain central issues in cosmology. These unresolved problems have motivated alternative approaches, such as dynamic dark energy models, where Λ evolves as a function of time, and interacting models, where dark energy interacts with other components in the cosmic fluid. In decaying vacuum energy models, Λ is not a constant; rather, it evolves over time and is thus a dynamic component $\Lambda(t)$. This approach addresses the fine-tuning problem by linking the present-day small value of Λ to its evolutionary trajectory during the Universe’s history. Early studies [14–29], often motivated by phenomenological considerations, laid the theoretical foundations and proposed certain functional forms of $\Lambda(t)$. More recently, many authors [30–37] have sought to ground these models in quantum field theory (QFT). This approach also works when Λ is considered to be a relic of inflationary dynamics [38].

Besides the dynamical $\Lambda(t)$ approach, recently, a new alternative to address late-time cosmic acceleration has gained traction. It is the ‘adiabatic’ matter creation which is gravitationally induced, and a non-equilibrium thermodynamical process. A long time ago, Schrödinger [39] conceptualized matter creation in the microscopic realm, which was further developed by Parker [40, 41]. Since Einstein’s field equations are the background equations to understand the evolution of the Universe, it was

* lokeshchander*23phdam04@dtu.ac.in

† cpsingh@dce.ac.in

Prigogine and his collaborators [42–44] who proposed a thermodynamic framework for open systems, allowing the creation of matter via transfer of energy from the gravitational field. In this case, by assuming that DM is being produced due to a time-varying gravitational field, it is plausible for a late-time acceleration to happen in a Universe consisting of only pressureless fluids, like cold dark matter and baryons. The research work carried out by many authors [45–61] suggests that matter creation can mimic the effects of dark energy, producing negative pressure and driving accelerated expansion. These models, rooted in thermodynamics, posit that new matter gets created as the Universe expands. With the energy conservation law, we suggest that this creation comes at the expense of another component in the cosmic fluid. When combined with DE characterized by a decaying vacuum term $\Lambda(t)$, there is a naturally arising coupling between the DE and matter sector, which consists of baryons and DM. The decay of $\Lambda(t)$ thus contributes to the creation of matter. While the exact mechanism of this phenomenon cannot be deduced, the implication is clear that DE and DM are interacting entities. This idea is somewhat similar to that of an exotic fluid like the Chaplygin gas (CG), which behaves like dark matter at early redshifts and like dark energy at later times. Many models based on various forms of the CG have been studied in the literature, and this approach has been promising since it is consistent with observational data [62–64]. Moreover, there are interacting dark energy (IDE) models in which interaction between the DE and other components in the cosmic fluid is assumed, and these models have been extensively explored in the literature. Along with the class of CG models, these models can solve the coincidence problem by allowing dark energy and dark matter to evolve over time. The gradual convergence of the two densities helps to resolve the issue of their seemingly fine-tuned values at present [65–68].

The present study investigates a combined model incorporating decaying vacuum energy and matter creation, offering a unified framework to address the aforementioned challenges. Unlike traditional interacting dark energy models that require an explicitly defined coupling term, this approach inherently links the decay of $\Lambda(t)$ to the rate of matter creation, denoted by Γ , avoiding the need for arbitrary assumptions about the form of coupling. To test the viability of the proposed model, we undertake a rigorous theoretical and observational analysis. With the help of Bayesian Markov Chain Monte Carlo (MCMC) methods, the model parameters are constrained with multiple datasets, including Baryon Acoustic Oscillations (BAO), Cosmic Microwave Background (CMB) distance priors, Pantheon Supernovae Type Ia (SNIa), $H(z)$ measurements from Cosmic Chronometers (CC), and weighted linear growth rate measurements $f(z)\sigma_8(z)$. Further, we employ statistical criteria; the reduced chi-squared test and two model selection criteria, AIC and BIC, which judge the model based on information theory and Bayesian statistics, respectively. This

allows for a robust comparison with the standard Λ CDM model, highlighting the potential advantages and limitations of the proposed framework.

The paper is organized in the following way: Section II lays down the groundwork for our cosmological model combining decaying vacuum energy with matter creation, outlining the modifications to the energy-momentum tensor and the Friedmann equations. In Section III, we present analytic solutions to the field equations, focusing on the following cosmological parameters: Hubble parameter $H(z)$, deceleration parameter $q(z)$, transitional redshift z_{tr} , and effective equation of state (EoS) parameter $w_{eff}(z)$. Section IV discusses perturbations in the cosmic background with primary focus on matter perturbations and their implications for structure formation. In Section V, we discuss the observational datasets and methodology employed for constraining the model, while in Section VI, we present the results of our analysis and discuss their cosmological implications. Section VII uses the reduced chi-squared test and two model selection criteria to compare our chosen model with a reference model, the Λ CDM Model. Then we focus on the thermodynamic analysis in Section VIII, where we proceed with finding an expression for the dark matter temperature. Then we calculate the total entropy of the universe and its evolution with respect to time, to test the generalized second law (GSL) of thermodynamics. Finally, in Section IX, we summarise our findings and the scope of future research.

II. DECAYING VACUUM MODEL WITH MATTER CREATION

Let us begin with a theoretical framework characterized by a spatially isotropic and homogeneous flat Friedmann-Lemaître-Robertson-Walker line element

$$ds^2 = -dt^2 + a^2(t) [dr^2 + r^2 (d\theta^2 + \sin^2 \theta d\phi^2)], \quad (1)$$

where (r, θ, ϕ) represents spherical coordinates and $a(t)$ is the scale factor, t denotes the cosmic time. Hereafter, we assume natural units $c = \hbar = 1$.

We introduce some basic thermodynamic concept of adiabatic matter creation as proposed by Prigogine and his collaborators [42–44] in cosmological context. We consider an N particle system under adiabatic conditions, which means that the total particle number changes and is not conserved. Mathematically, we express it as $N^\mu_{;\mu} \neq 0$. Due to this, the energy conservation equation gets modified. The particle flux vector, which measures how the particle number changes, is taken as $N^\mu = nu^\mu$, where $n = N/V$ gives the number of particles per unit of time (particle number density), and u^μ is the fluid’s four-velocity.

The non-conservation of the particle flux, i.e., $\nabla_\mu n^\mu = \psi$, can be written as

$$\dot{n} + 3Hn = \psi = n\Gamma, \quad (2)$$

where \dot{a} denotes derivative with respect to the cosmic time, $H = \dot{a}/a$ is the Hubble parameter and Γ quantifies the rate of change of the particle number in a physical volume V consisting N number of particles. Although the physical nature of Γ is unknown, we have one constraint over Γ , i.e., $\Gamma \geq 0$. For the generalized second law of thermodynamics to be valid, this must be true. Equation (2) gives the evolution of the particle number density. As the total number of particles per comoving volume a^3 is $N = a^3 n$, therefore, the above Eq.(2) can be written as $\dot{N}/N = \Gamma$. We define the entropy flux vector as $s^\mu = n\sigma u^\mu$, where σ is the entropy per particle. The entropy must satisfy the second law of thermodynamics, $s^\mu_{;\mu} \geq 0$. Also, we consider matter creation to be an adiabatic process, i.e., we have a system in which σ remains constant.

As we are assuming the total particle number N to be variable, we have a modification of the first law of thermodynamics:

$$d(\rho V) + p dV - \left(\frac{h}{n}\right) d(nV) = 0, \quad (3)$$

where ρ is the energy density and p is the equilibrium pressure of the cosmic matter fluid (dark matter and baryonic matter), and $h = (\rho + p)$ is the enthalpy per unit volume. We observe there to be an extra contribution in (3), and we interpret this as a non-thermal pressure arising due to the particle production process. We call this the ‘creation pressure’ p_c , which is given in terms of the change in particle number with respect to volume by

$$p_c = -\frac{h}{n} \frac{d(nV)}{dV}. \quad (4)$$

The negative sign indicates that p_c can help drive the accelerated cosmic expansion era. For simplicity’s sake, we assume that only dark matter particles are produced since the production of baryons is limited by the local gravity measurement-induced constraints.

From (2) and (4), along with the modified first law in (3), we obtain the following form of the creation pressure [44, 45, 61]:

$$p_c = -(\rho + p) \frac{\Gamma}{3H}. \quad (5)$$

Let us outline the fundamental equations of a general cosmological scenario. The gravitational field equations in Einstein’s General Relativity are:

$$G_{\mu\nu} = \kappa \tilde{T}_{\mu\nu}, \quad (6)$$

where $G_{\mu\nu} = R_{\mu\nu} - \frac{1}{2}g_{\mu\nu}R$ is the Einstein tensor which describes the spacetime geometry and κ is the Einstein gravitational constant which in this case is, $\kappa = 8\pi G/c^4 = 1$ due to the choice of units. $\tilde{T}_{\mu\nu} \equiv T_{\mu\nu} + g_{\mu\nu}\rho_\Lambda$ is the total energy-momentum tensor, which accounts for the contribution of both matter creation and a time-dependent vacuum term. In the presence of matter creation, it is customary to associate the creation pressure,

p_c in energy-momentum tensor. As a result, the usual perfect fluid energy-momentum tensor, $T_{\mu\nu}$ gets modified to

$$T_{\mu\nu} = (\rho_m + \tilde{p}_m) u_\mu u_\nu + g_{\mu\nu} \tilde{p}_m, \quad (7)$$

where u_μ is the four-velocity of the matter fluid, ρ_m is the matter energy density, and \tilde{p}_m is the total pressure exerted by the fluid which is the sum of the isotropic pressure p_m and the creation pressure p_c . We assume matter to be dust-like, i.e. it has negligible pressure ($p_m = 0$). In this paper, we assume that the vacuum behaves like a perfect fluid, with an equation of state given by $\rho_\Lambda = -p_\Lambda$. Given these considerations, we can write the Friedmann equations as follows:

$$3H^2 = \rho_m + \rho_\Lambda, \quad (8)$$

$$2\dot{H} + 3H^2 = -(p_c + p_\Lambda), \quad (9)$$

where $H = \dot{a}/a$ gives the expansion rate and is called the Hubble parameter. The conservation of the energy-momentum tensor, $\nabla^\mu \tilde{T}_{\mu\nu} = 0$ gives

$$\dot{\rho}_m + \dot{\rho}_\Lambda + 3H(\rho_m + \rho_\Lambda + p_c + p_\Lambda) = 0. \quad (10)$$

Since $\rho_\Lambda = -p_\Lambda$, the equation (10) gets simplified to:

$$\dot{\rho}_m + 3H(\rho_m + p_c) = -\dot{\rho}_\Lambda. \quad (11)$$

From (8) and (11), we can write the evolution equation as

$$2\dot{H} + 3H^2 + p_c = \rho_\Lambda. \quad (12)$$

III. SOLUTION OF THE FIELD EQUATIONS

In this section, we find the solution of the evolution equation (12) to constrain the parameters and discuss the results accordingly. Equation (12) can be solved for H if we know ρ_Λ , and Γ which gives us p_c through Eq. (5). Parametrization of Λ has changed over time and some in particular are: $\Lambda \propto a^{-2}$ [69], $\Lambda \propto a^{-m}$ [70] and $\Lambda \propto H^2$ [71]. Although there is no correct form for the decaying VED, it is often assumed as a function of the scale factor a or the expansion rate H . The motivation for taking it as a function of H is based on a quantum field theory (QFT) approach [72, 73]. This has been proposed in the context of the renormalization group (RG) [29, 74–76]. The interesting work by Shapiro and Solà [19], further investigated by many authors [37, 77–79] motivates us to adopt the following parametrization for the vacuum energy density:

$$\rho_\Lambda = c_0 + 3\nu H^2, \quad (13)$$

where c_0 is a constant term, and ν is an independent term associated with the vacuum decay. We expect ν to

be very small ($|\nu| \ll 1$) and interpret it as a perturbation term. In the limit $\nu \rightarrow 0$, the vacuum energy density becomes a constant, i.e. it reduces to the cosmological constant. This form is well motivated from the theoretical point of view as this is related to the general form of the effective action of QFT in curved spacetime.

In the proposed model, the cosmic history is based on the rate of expansion given by H and the evolution of energy density, which can define the gravitational creation rate Γ . This is often expressed as function of the expansion rate H , i.e. $\Gamma = \Gamma(H)$. The simplest form, though, would be taking Γ as a constant; $\Gamma = \Gamma_0$ and for matter creation to take place, this would be constrained by $\Gamma_0 > 0$. A direct proportionality to H can give us another form of the creation rate. In this paper, we consider a simple form that scales directly with the Hubble parameter [47] as

$$\Gamma = 3\beta H. \quad (14)$$

The parameter β is associated with the particle production. It is important to note that the matter creation rate Γ drops to zero in the limit $\beta \rightarrow 0$, meaning that the standard model with matter conservation (no creation or annihilation) is restored. Thus, like ν , it acts as a perturbation and therefore its value is expected to be small and positive.

Since we propose that our framework is interacting, we write the continuity equations for the matter and vacuum components in the following way:

$$\dot{\rho}_m + 3H(1 - \beta)\rho_m = Q, \quad \dot{\rho}_\Lambda = -Q. \quad (15)$$

Here Q is the interaction term, and its expression comes directly from the vacuum decay as

$$Q = -6\nu\dot{H}H. \quad (16)$$

The sign of Q determines the direction of energy flow. In the proposed scenario, vacuum energy decaying into dark matter is plausible because it aligns with particle production. Moreover, a model where the energy flow is in the opposite direction is generally not viable, [80] and therefore, we must ensure that Q is positive. We note that $Q \propto -6\dot{H}H = -(\dot{\rho}_m + \dot{\rho}_\Lambda)$ and ν in addition to being the vacuum decay parameter also determines the strength of the interaction. For the vacuum to act as a source, we must have $Q > 0$, and since \dot{H} is negative, the viability condition gives us $\nu > 0$. Additionally, from the above, we interpret matter to have an effective equation of state $w_m = -\beta$ due to the adiabatic matter creation process, which indicates a small deviation in behavior from a dust-like fluid.

Using (13) and (14) into (12), we obtain

$$\dot{H} + \frac{3}{2}(1 - \beta)(1 - \nu)H^2 = 3H_0^2(1 - \beta)(\Omega_\Lambda - \nu), \quad (17)$$

where $c_0 = 3H_0^2(\Omega_\Lambda - \nu)$, H_0 is the value of H at present and is called the Hubble constant, and Ω_Λ is

the present value of the dark energy density parameter. Equation(17) is a differential equation in H with respect to cosmic time t . Instead of using the variable t , it is more convenient to write the above equation in terms of the scale factor a or redshift z . Thus, Eq. (17) can be rewritten as

$$\frac{dH^2}{da} + \frac{3}{a}(1 - \beta)(1 - \nu)H^2 = \frac{3}{a}(1 - \beta)(\Omega_\Lambda - \nu)H_0^2. \quad (18)$$

The solution of (18) is given by

$$H(z) = H_0 \left[\left(1 - \frac{\Omega_\Lambda - \nu}{1 - \nu} \right) (1 + z)^{3(1 - \beta)(1 - \nu)} + \frac{\Omega_\Lambda - \nu}{1 - \nu} \right]^{1/2}, \quad (19)$$

where $(1 + z) = a_0/a(t)$. Here, a_0 represents the current cosmic scale factor value, typically assumed to be 1. The above expression gives the expansion rate in terms of the four independent model parameters H_0 , Ω_Λ , ν and β . Since we have considered only matter and vacuum components to be part of the cosmic fluid, we have $\Omega_m + \Omega_\Lambda = 1$.

From (19), the *scale factor* in terms of t can be found as

$$a = \left[\sqrt{\frac{\tilde{\Omega}_m}{\tilde{\Omega}_\Lambda}} \sinh \left(\frac{3}{2} \sqrt{\tilde{\Omega}_\Lambda} (1 - \beta)(1 - \nu) H_0 t \right) \right]^{\frac{2}{3(1 - \beta)(1 - \nu)}}, \quad (20)$$

where $\tilde{\Omega}_m = 1 - \frac{\Omega_\Lambda - \nu}{1 - \nu}$ and $\tilde{\Omega}_\Lambda = \frac{\Omega_\Lambda - \nu}{1 - \nu}$ are the effective fractional density parameters.

To discuss the decelerating and accelerating phases of the expansion of the Universe, along with the transition, we study the cosmological parameter known as the *deceleration parameter*, q , which is defined as:

$$q = -\frac{\ddot{a}}{aH^2} = -\left(1 + \frac{\dot{H}}{H^2} \right). \quad (21)$$

The equation (19) is used for obtaining an expression for the above, and it comes out to be:

$$q(z) = -1 + \frac{3(1 - \beta)(1 - \nu)\tilde{\Omega}_m(1 + z)^{3(1 - \beta)(1 - \nu)}}{\tilde{\Omega}_m(1 + z)^{3(1 - \beta)(1 - \nu)} + \tilde{\Omega}_\Lambda}. \quad (22)$$

The value of the deceleration parameter at present time, q_0 is given by

$$q_0 = -1 + \frac{3}{2}(1 - \beta)(1 - \Omega_\Lambda), \quad (23)$$

In late times, as we approach the present epoch $z = 0$, the deceleration parameter transitions from a positive to a negative value. This can be probed with another quantity called the *transitional redshift*. The expression for it is given by

$$z_{tr} = -1 + \left[\frac{2(\Omega_\Lambda - \nu)}{(1 - \Omega_\Lambda)(3(1 - \beta)(1 - \nu) - 2)} \right]^{\frac{1}{3(1 - \beta)(1 - \nu)}}. \quad (24)$$

Another key quantity that helps us understand the dynamics and the evolution of content in the Universe is the *effective equation of state* parameter w_{eff} . In this work, we have assumed that the decaying vacuum has an EoS parameter equal to -1 . We will now compute the model's effective EoS, which includes both decaying VED and matter with dark matter creation. This is calculated by the expression,

$$w_{\text{eff}} = -1 - \frac{2}{3} \frac{\dot{H}}{H^2}. \quad (25)$$

On substituting the relevant values into (25), we determine the effective EoS parameter to be as follows:

$$w_{\text{eff}}(z) = -1 + \frac{(1-\beta)(1-\nu)\tilde{\Omega}_m(1+z)^{3(1-\beta)(1-\nu)}}{\tilde{\Omega}_m(1+z)^{3(1-\beta)(1-\nu)} + \tilde{\Omega}_\Lambda}, \quad (26)$$

The present value of w_{eff} which we denote by w_0 , is given by

$$w_0 = -1 + (1-\beta)(1-\Omega_\Lambda). \quad (27)$$

IV. PERTURBATIONS IN THE COSMIC BACKGROUND

This section gives a general overview of cosmic perturbation theory in the context of a matter creation cosmology with a decaying vacuum. Studying cosmic perturbations is crucial, as they underpin the formation of large-scale structures in the Universe—such as stars, galaxies, clusters, and quasars. The reader is referred to the Refs.[81–84] for a detailed discussion on the theory of cosmological perturbations and the derivation of the perturbation equations. Here, we present only the basic equations and terms that are appropriate and relevant to our discussion.

The differential equation for the matter density contrast, defined as $\delta_m \equiv \delta\rho_m/\rho_m$, in the considered model can be approximated as follows [85]

$$\delta_m'' + \left(3 + a \frac{H'(a)}{H(a)}\right) \frac{\delta_m'}{a} - \frac{3}{2} \Omega_m(a) \frac{\delta_m}{a^2} = 0, \quad (28)$$

where ‘prime’ denotes differentiation with respect to the scale factor a . This second-order differential equation describes the evolution of the density contrast, as the primary effects arise from the specific form of the Hubble function.

To solve (28), we use the initial condition given in Ref.[86] as

$$\delta_{mi} = 1.5 \times 10^{-4} \quad \text{at} \quad a_i = 10^{-3}, \quad \text{and} \quad \delta'_{mi} = \delta_{mi}/a_i. \quad (29)$$

The expression for $\Omega_m(a)$ in terms of the model parameters can be derived through $\Omega_m(a) = 1 - \Omega_\Lambda(a)$, where

$$\Omega_\Lambda(a) = \frac{\rho_\Lambda}{3H^2} = \frac{\Omega_\Lambda - \nu}{E(a)^2} + \nu. \quad (30)$$

Here $E(a) = H(a)/H_0$ is the dimensionless Hubble parameter in terms of the scale factor $a = (1+z)^{-1}$. We substitute the required values into (28), allowing us to numerically compute the matter density contrast δ_{mi} using the initial conditions (29). Next, we consider the linear growth rate of δ_{mi} . This quantity is denoted by f , and in the linear theory, it is related to the peculiar velocity [87]. We define this as

$$f(a) = \frac{d \ln D_m(a)}{d \ln a}, \quad (31)$$

where $D_m(a) = \frac{\delta_m(a)}{\delta_m(a=1)}$ represents the linear growth function. The quantity denoted by $f\sigma_8$, called the ‘weighted linear growth rate’, is obtained by multiplying the linear growth rate $f(z)$, defined in (31), and $\sigma_8(z)$. Here, σ_8 is a parameter that measures the density root-mean-square fluctuation on $8h^{-1}$ Mpc scales [88, 89]. It is defined as [90]

$$\sigma_8(z) = \frac{\delta_m(z)}{\delta_m(z=0)} \sigma_8(z=0). \quad (32)$$

Using (31) and (32), the weighted linear growth rate is computed by the following relation:

$$f\sigma_8(z) = -(1+z) \frac{\sigma_8(z=0)}{\delta_m(z=0)} \frac{d\delta_m}{dz}. \quad (33)$$

V. DATA AND METHODOLOGY

In this section, we consider the well-established and most recent observational samples to constrain the model parameters. We use the Bayesian Markov Chain Monte Carlo (MCMC) method for statistical analysis, which is conducted using the *emcee* package in Python. Optimization of the best fit of parameters is done by maximization of the probability function given by

$$\mathcal{L} \propto \exp(-\chi^2/2), \quad (34)$$

where χ^2 is the chi-squared function. We enlist the χ^2 function for different data samples in the following subsections.

A. Sample of Type Ia supernovae (SNIa)

Often referred to as “standard candles,” SNIa are among the most popular cosmological probes used to study the Universe’s evolution. These supernovae are extremely luminous, with their peak brightness often rivalling that of their host galaxy [91]. Increasingly precise data from SNIa have solidified the original ground-breaking observations and their implications for the expansion of the universe[92–96].

The comprehensive Pantheon sample, which includes luminosity distance measurements of 1048 supernovae

across a redshift range of $0.01 < z < 2.26$, is used in this analysis. The observations allow us to constrain cosmological models using the observed distance modulus, μ_{obs} . The χ^2 of the SNIa dataset is defined as

$$\chi_{\text{SNIa}}^2 = \sum_{i=1}^{1048} \Delta\mu^T C^{-1} \Delta\mu, \quad (35)$$

where $\Delta\mu = \mu_{\text{obs}} - \mu_{\text{th}}$. Here, μ_{obs} represents the observed distance modulus, defined as

$$\mu_{\text{obs}} = m_B - M, \quad (36)$$

where m_B denotes the observed peak magnitude in the rest-frame B -band, and M gives the absolute B -band magnitude of a fiducial SNIa. We take the value of the magnitude M to be $M = -19.38$. The theoretical distance modulus, μ_{th} , is defined as

$$\mu_{\text{th}}(z, p) = 5 \log_{10} \left(\frac{D_L(z_{\text{hel}}, z_{\text{cmb}})}{1 \text{ Mpc}} \right) + 25, \quad (37)$$

where p represents the parameter space, which varies across different cosmological models, and D_L is the luminosity distance, expressed as

$$D_L(z_{\text{hel}}, z_{\text{cmb}}) = (1 + z_{\text{hel}})r(z_{\text{cmb}}). \quad (38)$$

The comoving distance $r(z)$ is calculated as

$$r(z) = cH_0^{-1} \int_0^z \frac{dz'}{E(z', p)}, \quad (39)$$

where $E(z) = H(z)/H_0$ is the dimensionless Hubble parameter, c is the speed of light in vacuum, and H_0 is the Hubble constant. The CMB-frame and heliocentric redshifts are denoted by z_{cmb} and z_{hel} , respectively. The covariance matrix C used in the χ^2 calculation is given by

$$C = D_{\text{stat}} + C_{\text{sys}}, \quad (40)$$

where D_{stat} is a diagonal matrix representing statistical uncertainties, and C_{sys} is the covariance matrix accounting for systematic uncertainties.

B. Baryon Acoustic Oscillations

The measurement of the background expansion history of the Universe can be achieved through the standard ruler provided by the imprint of Baryon Acoustic Oscillations (BAO). The BAO method has been extensively studied and validated in numerous works [97–99], providing a critical tool for constraining cosmological models. For a comprehensive discussion, the reader is referred to these studies. We present the basic equations and terms necessary for working with BAO measurements.

The comoving sound horizon is given by

$$r_s(z) = \frac{c}{H_0} \int_z^\infty \frac{c_s}{E(z')} dz', \quad (41)$$

where c is the speed of light in vacuum and c_s is the speed of sound, given by

$$c_s = \frac{1}{\sqrt{3(1 + R_b a)}}, \quad (42)$$

where R_b gives the baryon to photon density ratio, calculated as

$$R_b a = \frac{3\rho_b}{4\rho_\gamma}, \quad R_b = 31500 \omega_b \left(\frac{T_{\text{CMB}}}{2.7 \text{ K}} \right)^{-4}. \quad (43)$$

Here, $\omega_b = \Omega_b h^2$ is the baryon density parameter with $h = H_0/100$, and T_{CMB} is the current measured value of the CMB temperature.

One crucial period in our cosmic history is the baryon drag epoch, which refers to the time when baryons decoupled from photons. The redshift at drag epoch is calculated by the fitting function:

$$z_d = \frac{1345 \omega_m^{0.251}}{1 + 0.659 \omega_m^{0.828}} \left(1 + b_1 \omega_b^{b_2} \right), \quad (44)$$

where $b_1 = 0.313 \omega_m^{-0.419} (1 + 0.607 \omega_m^{0.674})$ and $b_2 = 0.238 \omega_m^{0.223}$. Here $\omega_m = \Omega_m h^2$ is the matter density parameter. By evaluating Eq. (41) at the drag epoch redshift z_d , we obtain a key quantity r_d which is a crucial term in BAO measurements. This gives the maximum distance sound waves could travel in the early Universe till the time of the last scattering (before the photon-baryon decoupling).

We use the latest BAO measurements from the Dark Energy Spectroscopic Instrument (DESI). The 12 data points used have been shown in Table I. The complete data, along with the survey details, can be found in Ref.[100, 101]. We constrain the model parameters from the BAO data using three observable within the redshift range $0.295 \leq z \leq 2.330$.

The first observable is the comoving angular distance $D_M(z)$ which is given by

$$D_M(z) = \int_0^z \frac{c}{H(z')} dz'. \quad (45)$$

Then we have the Hubble distance parameter $D_H(z)$ which is given by

$$D_H(z) = \frac{c}{H(z)}. \quad (46)$$

From the former two, we calculate the angle-average distance, which is given by

$$D_V(z) = (z D_M(z)^2 D_H(z))^{1/3}. \quad (47)$$

These quantities are normalized by the sound horizon r_d , which provides a standard ruler for measuring on large

TABLE I. Summary of tracer redshift and other observable parameters from the latest DESI BAO 2024 survey. The complete data is available at [101]

Tracer	Redshift Range	z_{eff}	D_M/r_d	D_H/r_d	D_V/r_d
BGS	0.1 - 0.4	0.295	—	—	7.93 ± 0.15
LRG1	0.4 - 0.6	0.510	13.62 ± 0.25	20.98 ± 0.61	—
LRG2	0.6 - 0.8	0.706	16.85 ± 0.32	20.08 ± 0.60	—
LRG3+ELG1	0.8 - 1.1	0.930	21.71 ± 0.28	17.88 ± 0.35	—
ELG2	1.1 - 1.6	1.317	27.79 ± 0.69	13.82 ± 0.42	—
QSO	0.8 - 2.1	1.491	—	—	26.07 ± 0.67
Lya QSO	1.77 - 4.16	2.330	39.71 ± 0.94	8.52 ± 0.17	—

scales. Thus, we calculate our theoretical values against the observed values D_M/r_d , D_H/r_d and D_V/r_d obtained from the BAO measurements, which can be referred to from Table I. The χ^2 functions for the BAO data are:

$$\chi_{D_M/r_d}^2 = \sum_{i=1}^5 \frac{(D_M(z_i, p) - D_{M,\text{obs}}(z_i))^2}{\sigma_{D_M}^2(z_i)}, \quad (48)$$

$$\chi_{D_H/r_d}^2 = \sum_{i=1}^5 \frac{(D_H(z_i, p) - D_{H,\text{obs}}(z_i))^2}{\sigma_{D_H}^2(z_i)}, \quad (49)$$

$$\chi_{D_V/r_d}^2 = \sum_{i=1}^2 \frac{(D_V(z_i, p) - D_{V,\text{obs}}(z_i))^2}{\sigma_{D_V}^2(z_i)}, \quad (50)$$

where $D_M(z_i, p)$, $D_H(z_i, p)$ and $D_V(z_i, p)$ are the theoretical values of the observable based on the model, and $D_{M,\text{obs}}$, $D_{H,\text{obs}}$ and $D_{V,\text{obs}}$ are the observed values of the DESI BAO measurements.

Thus, the total χ^2 value for the BAO data is

$$\chi_{BAO}^2 = \chi_{D_M/r_d}^2 + \chi_{D_H/r_d}^2 + \chi_{D_V/r_d}^2. \quad (51)$$

C. Cosmic Microwave Background

The Cosmic Microwave Background (CMB) measurements of the locations and amplitudes of peaks of acoustic oscillations give information about the distance to the surface of last scattering given by $r(z_*)$. This can be evaluated through Eq. (39) at z_* , which is the redshift at the time of recombination or last scattering. It marks the epoch when photons last scattered off free electrons before being able to freely travel through the universe, leaving behind their imprint in the form of the CMB radiation. The reader is referred to the Refs. [102, 103] for a more detailed discussion on CMB. We now proceed with the basic equations employed in the data analysis. The fitting function for recombination redshift z_* is

$$z_* = 1048 (1 + 0.00124 \omega_b^{-0.738}) (1 + g_1 \omega_m^{g_2}), \quad (52)$$

where

$$g_1 = \frac{0.0783 \omega_b}{1 + 39.5 \omega_b^{0.763}}, \quad g_2 = \frac{0.560}{1 + 21.1 \omega_b^{1.81}}. \quad (53)$$

Here ω_m and ω_b are the matter and baryon density parameters respectively. We are particularly interested in two quantities that characterize the CMB spectrum: the shift parameter and acoustic length scale.

It is observed that through the acoustic oscillations, doppler peaks are produced in the photon (radiation) spectrum. The placement of the peaks in the CMB spectrum is affected by the matter and radiation density, along with the dark energy. The shift in these peaks is probed by the shift parameter \mathcal{R} . The spectrum is affected in the line-of-sight direction, leading to the peak heights. We obtain \mathcal{R} through the relation:

$$\mathcal{R} = \sqrt{\Omega_m} H_0 \frac{r(z_*)}{c}. \quad (54)$$

The acoustic scale l_a determines the spacing between the peaks and characterizes the CMB temperature power spectrum in the transverse direction. This is calculated by

$$l_A = \frac{\pi r(z_*)}{r_s(z_*)}. \quad (55)$$

When working with CMB, we have to consider the radiation component as in early-times it was dominant. We use the relation $\Omega_r = \Omega_m/(1+z_{\text{eq}})$ to determine the radiation density, where z_{eq} is the epoch of matter-radiation equality and is given by

$$z_{\text{eq}} = 2.5 \times 10^4 \omega_m \left(\frac{T_{\text{CMB}}}{2.7 \text{ K}} \right)^{-4}, \quad (56)$$

where T_{CMB} represents the present-day temperature of the CMB. We adopt the best-fit value $T_{\text{CMB}} = 2.7255 \text{ K}$, measured by the COBE-FIRAS instrument [104]. CMB observation contribution in the constraint of cosmological parameters can be converted to CMB shift parameters for breaking degeneracy of parameters, instead of using the entire CMB power spectrum, [105, 106] This allows us to consider the data vector $\mathbf{v} = (R, l_A, \omega_b)^T$ which summarizes the Planck 2018 TT, TE, EE+lowE results [107]. The vector \mathbf{v} , along with the covariance matrix $C_{\mathbf{v}}$ have been reported in the Ref. [108].

The χ^2 function for the CMB data is given by:

$$\chi_{\text{CMB}}^2 = (\mathbf{v} - \mathbf{v}_{\text{th}})^T C_{\mathbf{v}}^{-1} (\mathbf{v} - \mathbf{v}_{\text{th}}), \quad (57)$$

where \mathbf{v}_{th} is the vector for the theoretical values of R, l_A, ω_b ; and $C_{\mathbf{v}}^{-1}$ is the inverse of the covariance matrix.

D. Sample of Cosmic Chronometer (CC)

The cosmic chronometer (CC) approach provides measurements of the Hubble parameter based on the galaxy differential age method using the largest galaxies that are passively evolving [109]. In our analysis, we use 32 CC data points from different surveys that span a redshift range of $0.07 \leq z \leq 1.965$. The χ^2 function for CC data is given by

$$\chi_{CC}^2 = \sum_{i=1}^{32} \frac{[H(z_i, p) - H_{\text{obs}}(z_i)]^2}{\sigma_H^2(z_i)}, \quad (58)$$

where $H(z_i, p)$ represents the theoretical value of the Hubble parameter for the model parameters, $H_{\text{obs}}(z_i)$ is the observed value of the Hubble parameter at redshift z_i , and $\sigma_H(z_i)$ is the associated uncertainty with $H_{\text{obs}}(z_i)$.

E. $f(z)\sigma_8(z)$ Data

We introduced the background evolution of matter perturbations in Section 4 and used Eq.(33) to define the weighted linear growth rate. To provide a more comprehensive analysis of the present model in the context of perturbation evolution, we focus on the observable quantity $f(z)\sigma_8(z)$. For this purpose, we use 18 data points from the "Gold" compilation, which contains measurements of $f(z)\sigma_8(z)$ obtained from various galaxy surveys. The data has been summarized in Table III of Ref. [110].

We compare the observational data with the theoretical values calculated from our models using the χ^2 function for $f(z)\sigma_8(z)$, which is defined as

$$\chi_{f\sigma_8}^2 = \sum_{i=1}^{18} \frac{[f\sigma_{8,\text{theo}}(z_i, p) - f\sigma_{8,\text{obs}}(z_i)]^2}{\sigma_{f\sigma_8}^2(z_i)}, \quad (59)$$

where $f\sigma_{8,\text{theo}}(z_i, p)$ is the theoretical value computed using (33), and $f\sigma_{8,\text{obs}}(z_i)$ represents the observed data.

Using three different combinations of the data discussed above, we employ Bayesian MCMC methods to explore the parameter space of the proposed model described in Section III, using the `emcee` Python package [111, 112]. We use the following chi-squared functions:

- **DS1:** This dataset consists of a combination of data from the observations of SNIa, BAO, and CMB. It contains 1063 independent data points. The total χ^2 function for this dataset is given by

$$\chi_{\text{tot}}^2 = \chi_{\text{SNIa}}^2 + \chi_{\text{BAO}}^2 + \chi_{\text{CMB}}^2. \quad (60)$$

- **DS2:** The first dataset is augmented with the cosmic chronometer (CC) data containing 32 data

points making the total to be 1095. In this case, the total χ^2 function is defined as

$$\chi_{\text{tot}}^2 = \chi_{\text{SNIa}}^2 + \chi_{\text{BAO}}^2 + \chi_{\text{CMB}}^2 + \chi_{H(z)}^2. \quad (61)$$

- **DS3:** We further expand DS2 by including the weighted linear growth rate data from the $f\sigma_8$ measurements. The total data points are 1113 and for this combination, the total χ^2 function becomes

$$\chi_{\text{tot}}^2 = \chi_{\text{SNIa}}^2 + \chi_{\text{BAO}}^2 + \chi_{\text{CMB}}^2 + \chi_{H(z)}^2 + \chi_{f\sigma_8}^2. \quad (62)$$

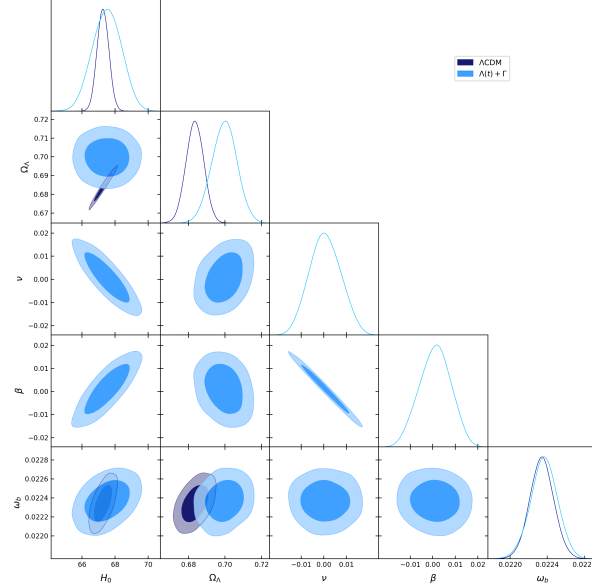
VI. RESULTS AND DISCUSSION

We now discuss over the outcomes from various data sets to constrain our model with Hubble parameter, given in Eq.(19). For the parameters of the Λ CDM and the $\Lambda(t) + \Gamma$ models, Figures 1-3 display the combined $1 - \sigma(68.3\%)$ and $2 - \sigma(95.4\%)$ confidence level (CL) contours with marginalized likelihood distributions. Table II displays the matching parameter constraints for the datasets DS1, DS2, and DS3 that were acquired from the MCMC sampler. The best fit values of Hubble constant for $\Lambda(t) + \Gamma$ come out to be $H_0 = 67.517 \pm 0.869$ km/s/Mpc for DS1 data, $H_0 = 67.534 \pm 0.874$ km/s/Mpc for DS2 data, and $H_0 = 67.533 \pm 0.884$ km/s/Mpc for DS3 data. We know that the discrepancies in the measurement of H_0 between the Planck collaboration [113] and independent cosmological probes [114] refer to H_0 tension. The Planck collaborator estimates $H_0 = 67.27 \pm 0.06$ km/s/Mpc, whereas R22 reported $H_0 = 73.04 \pm 1.04$ km/s/Mpc which leads to a tension of 4.89σ . Our estimated values of H_0 from three the datasets show very little tension with the Planck result upon comparison. We plot the evolution of $H(z)$ for Λ CDM and decaying VED with matter creation model using 32 data points of CC as shown in Figs. 4-6. Both models are in agreement for the three datasets, as the hybrid model and the standard model coincide for nearly the whole evolution period and the model paths cover most of the CC dataset with the error bars.

In Figs. 7-9, we present the evolution of the deceleration parameter with respect to redshift. The transition redshift z_{tr} at which the Universe transits from a decelerating phase to an acceleration phase occurs at $z_{\text{tr}} = 0.675 \pm 0.019$ with DS1, $z_{\text{tr}} = 0.675 \pm 0.019$ with DS2, and at $z_{\text{tr}} = 0.677 \pm 0.019$ with DS3 which doesn't vary much from the standard model but the transition happens earlier. The analysis shows that the Universe is currently in an accelerating phase of cosmic expansion, whereas it was in a decelerating phase in the past. We find the constraints of the present value of the deceleration parameter as $q_0 = -0.550 \pm 0.010$, -0.550 ± 0.010 and -0.551 ± 0.010 for DS1, DS2 and DS3 datasets, respectively. Comparing with the values of q_0 obtained for

TABLE II. Constraints on parameters for Λ CDM and $\Lambda(t) + \Gamma$ model for different observational data sets.

Parameter	DS1		DS2		DS3	
	Λ CDM	$\Lambda(t) + \Gamma$	Λ CDM	$\Lambda(t) + \Gamma$	Λ CDM	$\Lambda(t) + \Gamma$
H_0	67.278 ± 0.355	67.517 ± 0.869	67.301 ± 0.353	67.534 ± 0.874	67.993 ± 0.414	67.533 ± 0.884
Ω_Λ	0.68362 ± 0.00482	0.69973 ± 0.00685	0.68398 ± 0.00479	0.69989 ± 0.00684	0.69337 ± 0.00540	0.70035 ± 0.00680
ν	-	0.00069 ± 0.00692	-	0.00058 ± 0.00687	-	0.00067 ± 0.00694
β	-	0.00109 ± 0.00694	-	0.00122 ± 0.00685	-	0.00120 ± 0.00694
ω_b	0.02234 ± 0.00013	0.02237 ± 0.00014	0.02235 ± 0.00013	0.02237 ± 0.00015	0.02247 ± 0.00013	0.02237 ± 0.00014
σ_8	-	-	-	-	0.755 ± 0.026	0.762 ± 0.028
S_8	-	-	-	-	0.763 ± 0.026	0.762 ± 0.027
z_{tr}	0.629 ± 0.012	0.675 ± 0.019	0.630 ± 0.012	0.675 ± 0.019	0.654 ± 0.014	0.677 ± 0.019
q_0	-0.525 ± 0.007	-0.550 ± 0.010	-0.526 ± 0.007	-0.550 ± 0.010	-0.540 ± 0.008	-0.551 ± 0.010
w_0	-0.684 ± 0.005	-0.700 ± 0.007	-0.684 ± 0.005	-0.700 ± 0.007	-0.684 ± 0.005	-0.700 ± 0.007
t_0 (Gyr)	13.80 ± 0.02	13.98 ± 0.18	13.80 ± 0.02	13.98 ± 0.19	13.78 ± 0.02	13.99 ± 0.19

FIG. 1. The one-dimensional marginalized distribution and two-dimensional contour plots for Λ CDM and $\Lambda(t) + \Gamma$ models at 68.3% and 95.4% confidence levels using DS1 dataset.

the Λ CDM model, we see that the expansion of the Universe is accelerating at a slightly faster rate. Overall, the values of both q_0 and z_{tr} obtained for the model agree with the values obtained for the standard model.

In the considered cosmological scenario, the calculated values of the age of the Universe t_0 based on the parameter constraints obtained for the three datasets are 13.98 ± 0.18 Gyr, 13.98 ± 0.19 Gyr, and 13.99 ± 0.19 Gyr, respectively which when compared with the mean value for the standard model 13.79 ± 0.02 Gyr suggest a longer cosmic history however the difference is not that significant. This can be attributed to the perturbations through matter creation and vacuum decay. In this study, we have initially assumed the EoS of vacuum energy as $w_\Lambda = -1$. Therefore, we investigate the total effective EoS given by (26). The evolution of EoS is depicted in Figs. 10-12. It is obvious from the figures that w_{eff} has a negative value such that $w_{\text{eff}} < -1/3$, which indicates an accelerating phase in the expansion.

In the future, we can see that the model asymptotically approaches negative unity, i.e. $w_{\text{eff}} = -1$, implying complete vacuum domination. The present values of w_{eff} , represented by w_0 , strongly favor a value around -0.700 ± 0.007 across all three datasets for the presented model which indicates the transition towards a dark energy era. The values are also consistent with those reported for the Λ CDM model.(cf. Table II)

Let us now discuss σ_8 and S_8 , which are crucial for structure formation and are obtained by probing cosmological perturbations, as discussed in Section 4. The DS3 column in Table II reports the parameter constraints for these quantities. For the $\Lambda(t) + \Gamma$ model, we have $\sigma_8 = 0.762 \pm 0.028$, which is a good result considering the slight deviation with Λ CDM. We rephrase this in terms of the fitting value of the related LSS observable $S_8 = \sigma_8 \sqrt{\Omega_m}/0.3$, which gives $S_8 = 0.762 \pm 0.0297$. Comparing it with $S_8 = 0.763 \pm 0.026$ of Λ CDM model for the same DS3 dataset and $S_8 = 0.737 \pm 0.036$ of weak

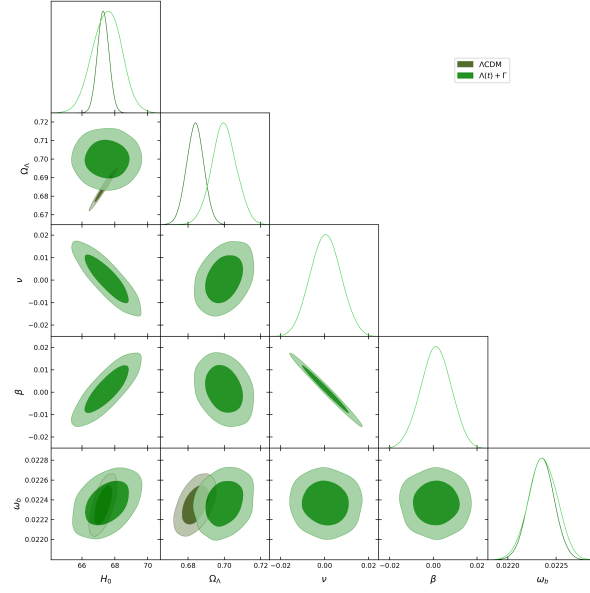


FIG. 2. The one-dimensional marginalized distribution and two-dimensional contour plots for Λ CDM and $\Lambda(t) + \Gamma$ models at 68.3% and 95.4% confidence levels using DS2 dataset.

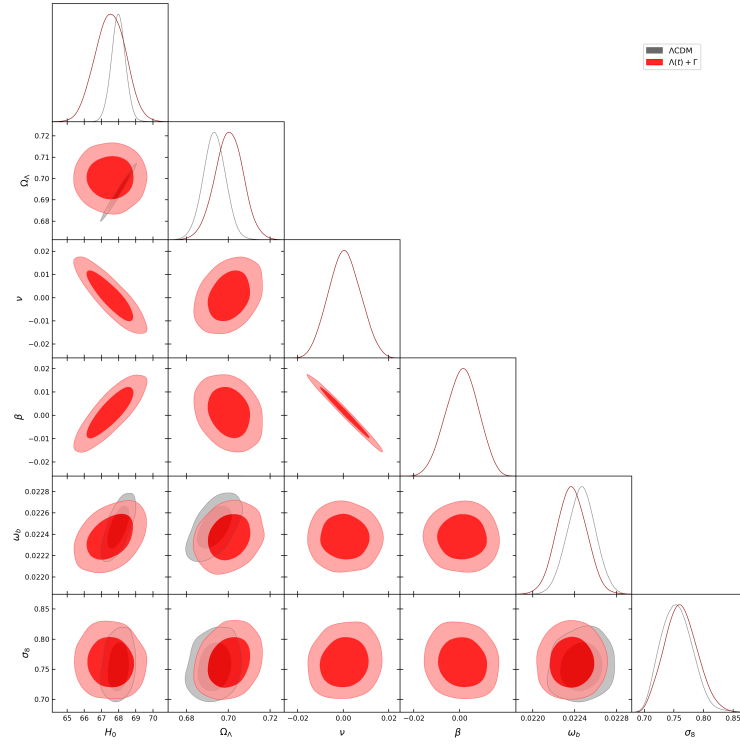


FIG. 3. The one-dimensional marginalized distribution and two-dimensional contour plots for Λ CDM and $\Lambda(t) + \Gamma$ models at 68.3% and 95.4% confidence levels using DS3 dataset.

lensing measurement, we find that there is no residual tension left as mismatch is less than 1σ . We have also plotted $f(z)\sigma_8(z)$ data corresponding to both the standard model and our model in Fig. 13. We have used 18 data points from the $f(z)\sigma_8(z)$ Gold data along with

their uncertainty measures. The curves provide a fairly good fit for the data, implying our model agrees with the observational data in the context of structure formation and cosmic perturbations.

We have found that the best-fit values of decaying pa-

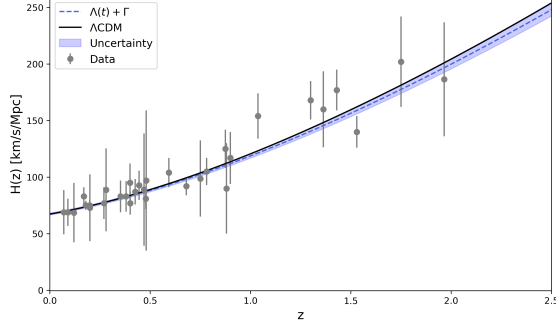


FIG. 4. Best-fit using DS1 over $H(z)$ data for the $\Lambda(t) + \Gamma$ model (blue dotted line) and standard model (black line). The shaded band represents the uncertainty for the former. The grey points with error bar represent the 32 CC data points.

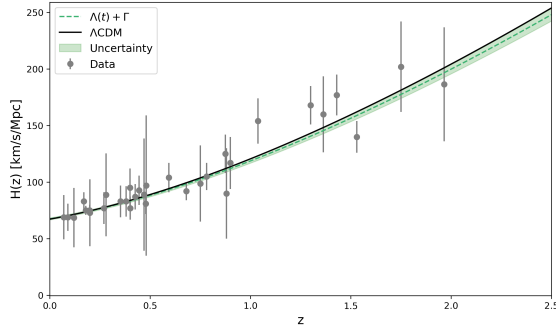


FIG. 5. Best-fit using DS2 over $H(z)$ data for the $\Lambda(t) + \Gamma$ model (green dotted line) and standard model (black line). The shaded band represents the uncertainty for the former. The grey points with error bar represent the 32 CC data points.

parameter are $\nu = 0.00069 \pm 0.00692$, $\nu = 0.00058 \pm 0.00687$ and $\nu = 0.00067 \pm 0.00694$, and of the matter creation parameter are $\beta = 0.00109 \pm 0.00694$, $\beta = 0.00122 \pm 0.00685$ and $\beta = 0.00120 \pm 0.00694$ using DS1, DS2 and DS3 datasets, respectively. The results confirm that these parameters act as a perturbation to the Λ CDM model.

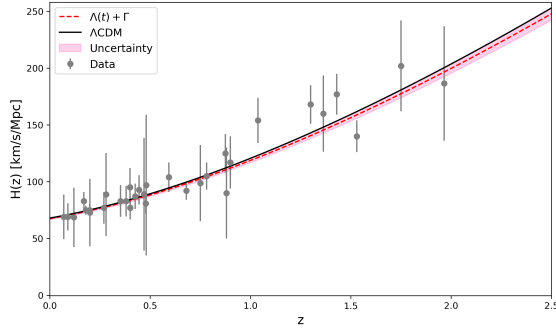


FIG. 6. Best-fit using DS3 over $H(z)$ data for the $\Lambda(t) + \Gamma$ model (red dotted line) and standard model (black line). The shaded band represents the uncertainty for the former. The grey points with error bar represent the 32 CC data points.

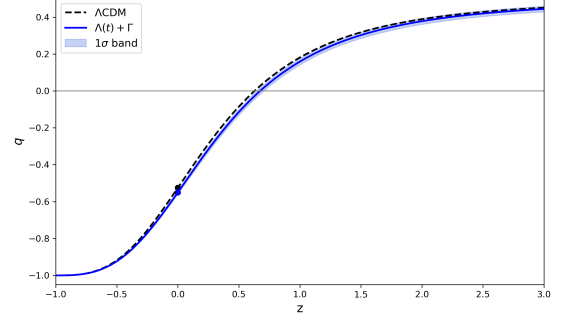


FIG. 7. The deceleration parameter versus redshift for the $\Lambda(t) + \Gamma$ model using DS1 dataset. The standard model's evolution is depicted by the dashed curve.

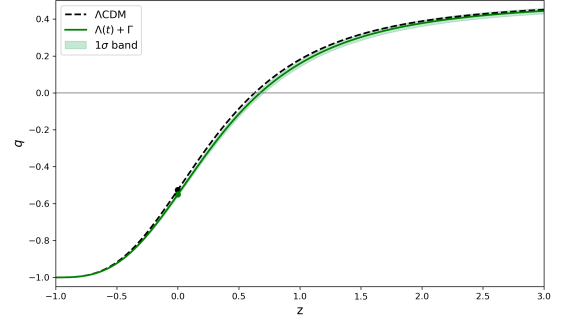


FIG. 8. The deceleration parameter versus redshift for the $\Lambda(t) + \Gamma$ model with DS2 dataset. The standard model's evolution is depicted by the dashed curve.

The values obtained for the baryon density parameter $\omega_b = \Omega_b h^2$ are also in good agreement with the Planck values across the three datasets.

Furthermore, we report the cosmographic parameter, known as the jerk parameter, which is defined by $j = \ddot{a}/aH$. It gives information about the dynamics of the DE EoS. In terms of the deceleration parameter, it is given by the expression:

$$j = q(2q + 1) + (1 + z) \frac{dq}{dz}. \quad (63)$$

It can be verified that for the standard model, the value of the jerk parameter is a constant, i.e. $j = 1$. This parameter is a dimensionless third derivative of the scale factor and can help us study how our model deviates from the standard model. For the proposed model, the jerk parameter (63) gives

$$j = 3(1 - \beta)(1 - \nu)(q + 1) - 3q - 2. \quad (64)$$

We see that in the limit where the model parameters β and ν are zero, j reduces to one. In the case of the deceleration parameter, negative values imply an

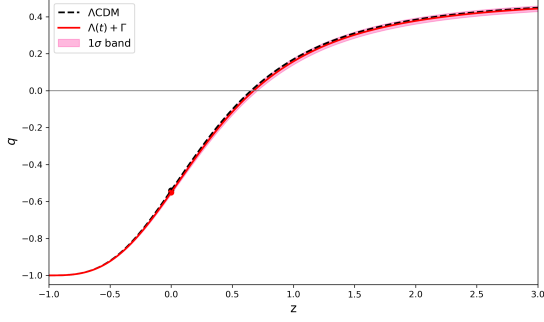


FIG. 9. The deceleration parameter versus redshift for the $\Lambda(t) + \Gamma$ model with DS3 dataset. The standard model's evolution is depicted by the dashed curve.

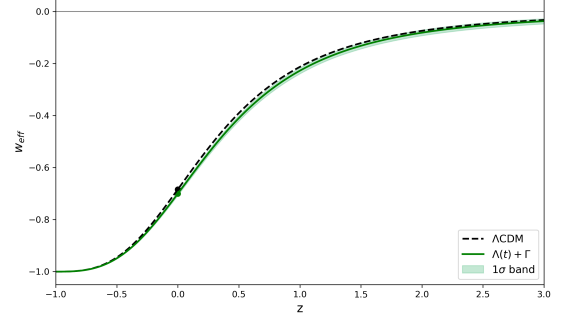


FIG. 11. Effective EoS parameter for the $\Lambda(t) + \Gamma$ model with DS2 as a function of redshift z . The standard model's evolution is depicted by the dashed curve.

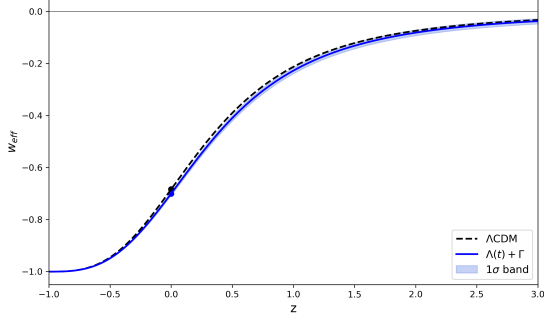


FIG. 10. Effective EoS parameter for the $\Lambda(t) + \Gamma$ model with DS1 as a function of redshift z . The standard model's evolution is depicted by the dashed curve.

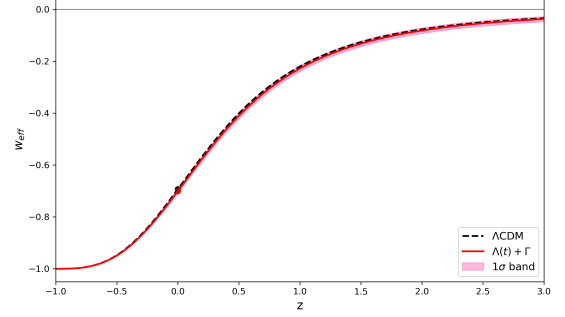


FIG. 12. Effective EoS parameter for the $\Lambda(t) + \Gamma$ model with DS3 as a function of redshift z . The standard model's evolution is depicted by the dashed curve.

accelerating expansion of the Universe. However, in the case of the jerk parameter, a positive value represents the same, and from (64), we can see that for the considered model, the value will remain positive. In Fig.14, the evolution of this parameter is shown for our model using the parameter constraints obtained for all three datasets. The figure confirms the positive nature, and we see that it remains close to but less than unity at early redshifts, eventually tending to 1 in the future. Thus, in the past, the parameter deviates from the standard model; however, in late time, it converges to a similar behaviour.

We also plot the evolution of matter density in Λ CDM and the proposed model in Fig.15 using the cosmological parameter estimates of DS1, DS2 and DS3 datasets. We consider a single case for the evolution in the case of the standard model represented by a black line. We see that in late time, the matter density tends towards zero for all the cases, resulting from the accelerated expansion causing complete vacuum domination. We also observe that because of our particular selection of the particle production rate, the creation pressure p_c , which contributes to this acceleration, has the expression

$p_c = -\beta\rho_m$. The evolution of this pressure is plotted in Fig.16, which shows that it increases from negative infinity at higher redshifts and converges towards zero in late time. Thus, particle production will cease in the dark energy domination era.

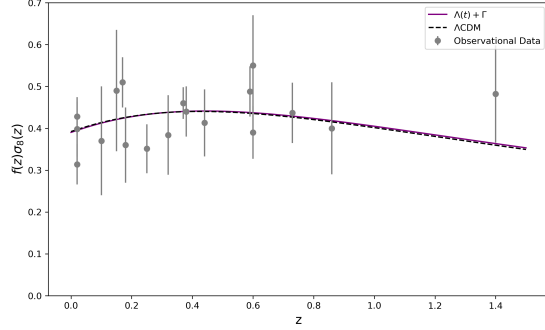
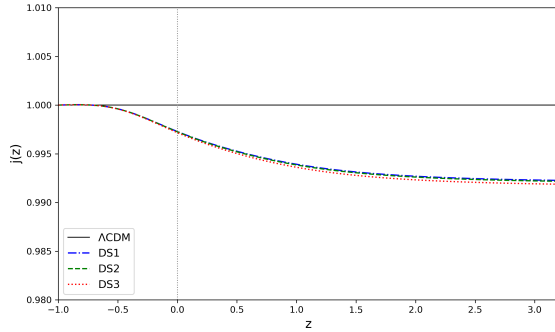
VII. SELECTION CRITERIA

In this section, we are interested in determining the models that could perform better with respect to the observational data used in the analysis. We utilize three selection statistical criteria, namely, reduced chi-squared, Akaike information criteria and Bayesian information criteria, which consider the presence of an extra degree of freedom.

Table III presents the χ^2 and the reduced χ^2 values for the standard model and the presented model, respectively. The reduced χ^2 , denoted by χ^2_{red} , is calculated by the formula $\chi^2_{red} = \chi^2/(N - d)$, where N is the total number of data points (here, it is 1063, 1095 and 1113 for DS1, DS2 and DS3, respectively), and d is the number of

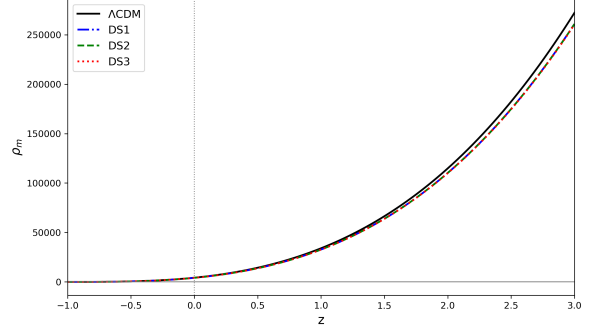
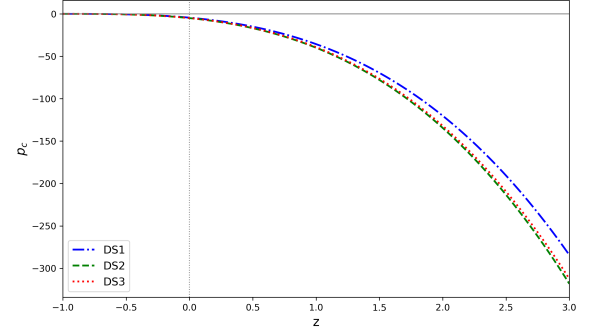
TABLE III. Comparison of χ^2 , AIC, and BIC values for Λ CDM and the $\Lambda(t) + \Gamma$ model across different datasets.

Values	DS1		DS2		DS3	
	Λ CDM	$\Lambda(t) + \Gamma$	Λ CDM	$\Lambda(t) + \Gamma$	Λ CDM	$\Lambda(t) + \Gamma$
χ^2	1057.31	1057.00	1072.26	1071.72	1085.06	1084.58
d	3	5	3	5	4	6
N	1063	1063	1095	1095	1113	1113
χ^2_{red}	0.997	0.999	0.982	0.983	0.978	0.980
AIC	1063.33	1067.06	1078.29	1081.78	1093.10	1096.65
BIC	1078.22	1091.85	1093.26	1106.72	1113.12	1126.66
ΔAIC	—	3.73	—	3.49	—	3.55
ΔBIC	—	13.63	—	13.46	—	13.54

FIG. 13. Theoretical curves for the $f(z)\sigma_8(z)$ data corresponding to the standard model and the $\Lambda(t) + \Gamma$ model obtained from the parameter constraints for the cosmological parameters.FIG. 14. Jerk parameter j with redshift z using parameter constraints obtained for the $\Lambda(t) + \Gamma$ model. The black line depicts the value for the standard model, i.e. 1.

free parameters ($d = 3$ for Λ CDM and $d = 5$ for $\Lambda(t) + \Gamma$ model for DS1 and DS2, and one additional parameter σ_8 is added to both for DS3). It is to be noted that a reduced χ^2 value less than one gives a good fit, and greater than one indicates a poor fit. From Table III, we see that the reduced χ^2 values are less than 1, indicating that our model fits well with the observational datasets and the data fits well with the current models. This is just one criterion to test the viability of our model. We will utilize two selection criteria for further analysis.

The Akaike information criteria (AIC) value is calcu-

FIG. 15. Plot of matter density with the redshift z for the $\Lambda(t) + \Gamma$ corresponding to the three combined datasets. The black line represents the evolution of the standard model.FIG. 16. Evolution of the creation pressure with redshift z corresponding to the three different datasets. The pressure eventually tends towards zero in the future.

lated as [115]

$$AIC = \chi^2_{\min} + \frac{2d N}{N - d - 1}, \quad (65)$$

where χ^2_{\min} is the minimum value of the χ^2 -function. Equation(65) makes it clear that the penalty for the extra number of free parameters is represented by the second term on the right hand side. In cases where d is significantly lesser than N , Eq.(65) reduces to $AIC = \chi^2_{\min} + 2d$. To test the proposed model M_1 against the reference model M_0 , we calculate the difference in their respective AIC values as $\Delta AIC_{M_1 M_0} = AIC_{M_1} - AIC_{M_0}$,

which is interpreted as the "evidence in favour" of the model M_1 as compared to the reference M_0 . In this paper, the concordance model has been considered as the reference.

The value $0 \leq AIC_{M_1 M_0} < 2$ indicates "strong evidence in favour" of the proposed model M_1 . For $2 \leq AIC_{M_1 M_0} \leq 4$, there is "averagely strong evidence in favour" of M_1 . If $4 < AIC_{M_1 M_0} \leq 7$, then there is "little evidence in favour", whereas for $AIC_{M_1 M_0} > 7$, there is "no evidence in favour" of the proposed model.

On the other hand, the Bayesian information criterion (BIC) is defined as [116]

$$BIC = \chi_{min}^2 + d \ln N \quad (66)$$

Likewise $\Delta AIC_{M_1 M_0}$, we compute $\Delta BIC_{M_1 M_0}$ as $\Delta BIC_{M_1 M_0} = BIC_{M_1} - BIC_{M_0}$. This gives the "evidence against the model M_1 with respect to the reference model M_0 ". Thus, the ranges of the values for BIC and their interpretation are different from those of AIC. The value $0 \leq BIC_{M_1 M_0} < 2$ indicates "not enough evidence in favour" of the proposed model M_1 . For $2 \leq BIC_{M_1 M_0} < 6$, there is "evidence against" the model M_1 , and for $6 \leq BIC_{M_1 M_0} < 10$, we have "strong evidence against" model M_1 . If $BIC_{M_1 M_0} \geq 10$ then there is "overwhelmingly strong evidence" against the proposed model, and it is not the best model.

The values of $\Delta AIC_{M_1 M_0}$ and $\Delta BIC_{M_1 M_0}$ are shown in Table III. For the three datasets, DS1, DS2 and DS3, we obtain $\Delta AIC_{M_1 M_0}$ values to be 3.73, 3.49, and 3.55, respectively, indicating averagely strong evidence in favour of our proposed model with respect to the standard model for all the datasets. The $\Delta BIC_{M_1 M_0}$ values obtained for the datasets are 13.63, 13.46, and 13.54, respectively. This indicates that the evidence against our model is overwhelmingly strong and it is not the best fit for the data according to BIC.

VIII. THERMODYNAMIC ANALYSIS

In this section, we focus on the thermodynamic analysis of a universe under the proposed scenario. First we use the generalized first law of thermodynamics to obtain an expression for the dark matter temperature in terms of our model parameters. Then, we test the validity of generalized second law (GSL) of thermodynamics by computing the total entropy of the universe and its evolution w.r.t time and assess the results.

A. Dark Matter Temperature

Let us consider the modified first law of thermodynamics, given by Eq.(3). This can be rewritten as

$$d(\rho_m V) + \tilde{p}_m dV - \frac{(\rho_m + \tilde{p}_m)}{n} d(nV) = 0, \quad (67)$$

where $h = (\rho_m + \tilde{p}_m)$. Taking time derivative of Eq. (67), we have

$$\dot{\rho}_m = \frac{\dot{n}}{n}(\rho_m + \tilde{p}_m). \quad (68)$$

Since the temperature is defined by Gibbs equation

$$TdS = d\left(\frac{\rho_m}{n}\right) + \tilde{p}_m d\left(\frac{1}{n}\right) \quad (69)$$

We have $T = T(n, \rho_m)$ which gives

$$\dot{T} = \frac{\partial T}{\partial n} \dot{n} + \frac{\partial T}{\partial \rho_m} \dot{\rho}_m. \quad (70)$$

Using (68) into (70), we get

$$\dot{T} = \frac{\dot{n}}{n} \left[\frac{\partial T}{\partial n} n + \frac{\partial T}{\partial \rho_m} (\rho_m + \tilde{p}_m) \right]. \quad (71)$$

Using the integrability condition, $\partial^2 S / \partial T \partial n = \partial^2 S / \partial n \partial T$, one gets

$$\frac{\partial T}{\partial n} n + \frac{\partial T}{\partial \rho_m} (\rho_m + \tilde{p}_m) = T \frac{\partial \tilde{p}_m}{\partial \rho_m}. \quad (72)$$

Using (72) into (71), we obtain the evolution equation for the temperature which is given by

$$\frac{\dot{T}}{T} = \frac{\dot{n}}{n} \frac{\partial \tilde{p}_m}{\partial \rho_m} = w_{\text{eff}} \frac{\dot{n}}{n}. \quad (73)$$

Using Eq.(2) in above equation, we get

$$\frac{\dot{T}}{T} = -3w_{\text{eff}} H \left(1 - \frac{\Gamma}{3H} \right), \quad (74)$$

or equivalently,

$$\frac{\dot{T}}{T} = 3\beta(1 - \beta)H. \quad (75)$$

Using (20) into (75), we obtain the temperature of dark matter

$$T = T_0 \left[\sqrt{\frac{\tilde{\Omega}_m}{\tilde{\Omega}_\Lambda}} \sinh \left(\frac{3}{2} \sqrt{\tilde{\Omega}_\Lambda} (1 - \beta)(1 - \nu) H_0 t \right) \right]^{\frac{2\beta}{(1-\nu)}}. \quad (76)$$

Using (20) into (2) we can obtain the particle number density which is given by

$$n(t) = n(t_0) \left[\sqrt{\frac{\tilde{\Omega}_m}{\tilde{\Omega}_\Lambda}} \sinh \left(\frac{3}{2} \sqrt{\tilde{\Omega}_\Lambda} (1 - \beta)(1 - \nu) H_0 t \right) \right]^{-\frac{2}{(1-\nu)}}. \quad (77)$$

B. Generalized Second Law of Thermodynamics

This section is devoted to examine and analyse the validity of generalized second law (GSL) of thermodynamics for the presented model. According to the GSL of thermodynamics, the total entropy of the Universe, i.e., sum of the horizon entropy and entropy of the fluid always increases with time [117]. Mathematically, we can express it as

$$\frac{d}{dt}(S_H + S_m + S_\Lambda) \geq 0, \quad (78)$$

where S_H is the entropy associated with the Hubble horizon (apparent horizon) for flat Universe, S_m is the entropy of dark matter produced by gravitationally induced matter creation and S_Λ is the entropy associated with vacuum energy. The GSL thermodynamics was first formulated for black hole by Bekestein and Hawking [117]. They stated that the black hole horizons have entropy and temperature associated with them. According to Bekenstein, the horizon entropy is proportional to the area of the horizon, which is given by

$$S_H = \frac{k_B A}{4l_{Pl}^2}, \quad (79)$$

where k_B is the Boltzmann constant, $A = 4\pi R_H^2$ is the area of the Hubble horizon and $l_{Pl} = \sqrt{\frac{\hbar G}{c^3}}$ is the Planck length. Here, $R_H = \frac{1}{\sqrt{(H^2 + \kappa a^{-2})}}$ is the radius of the Hubble horizon. In a spatially flat FLRW Universe, we have $R_H = \frac{1}{H}$. Assuming $k_B = \hbar = c = 8\pi G = 1$, the above equation can be rewritten as

$$S_H = \frac{8\pi^2}{H^2} \quad (80)$$

Therefore, the rate of change of entropy of the Hubble horizon is given by

$$\dot{S}_H = -\frac{16\pi^2}{H^3} \dot{H} \quad (81)$$

The entropy of cosmic components (matter and dark energy) inside the Hubble horizon can be calculated by the Gibb's equation [118]

$$T dS = d(\rho V) + p dV, \quad (82)$$

where $V = 4\pi/3H^3$ is volume enclosed by horizon and T is temperature associated with both matter and dark energy and due to their mutual interaction, we assume that T is equal. We assume that the system bounded by the Hubble horizon remains in equilibrium so that the temperature distribution is uniform and its value equal to the temperature of the horizon. In this case, Gibbons-Hawking temperature, $T = H/2\pi$ is a natural choice for the horizon temperature. It is evident from (82) that the vacuum energy density in the present model doesn't

contribute to the entropy as $\rho_\Lambda = -p_\Lambda$. The non-zero contribution to the entropy is only due to dark matter produced by gravitationally induced matter creation, which is given by

$$S = \frac{(\rho_m + \tilde{p}_m)V}{T}, \quad (83)$$

where $\tilde{p}_m = p_m + p_c$. Substituting $V = 4\pi/3H^3$ and $T = H/2\pi$ in above equation, we get matter entropy as

$$S_m = \frac{8\pi^2}{3H^4}(\rho_m + p_c). \quad (84)$$

Using $p_c = -\beta\rho_m$, Equation (84) can be written as

$$S_m = \frac{8\pi^2(1-\beta)\rho_m}{3H^4}, \quad (85)$$

where matter energy density ρ_m is obtained from the Friedmann equation (8), which is given by

$$\rho_m = 3H_0^2(1-\nu)\tilde{\Omega}_m a^{-3(1-\beta)(1-\nu)}. \quad (86)$$

Using (80) and (85) the total entropy of the Universe, i.e., $S = S_H + S_m$ is calculated as

$$S = \frac{8\pi^2}{H^2} \left[1 + \frac{(1-\beta)\rho_m}{3H^2} \right]. \quad (87)$$

On substituting the value of ρ_m from (86), we see that the total entropy can be simplified in terms of deceleration parameter q , given in (22), as

$$S = \frac{8\pi^2}{3H^2}(5+2q). \quad (88)$$

Now, to check the validity of GSL, given by (78) for this model, we have the combined change in entropy for the dark fluid

$$\dot{S}_m = -\frac{8\pi^2(1-\beta)\rho_m}{H^3} \left(1 + \frac{\dot{H}}{H^2} \right). \quad (89)$$

Combining (81) and (89), and noting Eq. (21), we obtain the total change in entropy as

$$\dot{S} = \frac{8\pi^2}{H} \left[2(1+q) + \frac{(1-\beta)\rho_m}{H^2} q \right], \quad (90)$$

in which we substitute the value of ρ_m and solve further to obtain the simplified expression

$$\dot{S} = \frac{16\pi^2}{H}(1+q)^2. \quad (91)$$

In equation (91) it is noted that $\dot{S} \geq 0$ as all the terms are positive and hence the GSL is satisfied. In the asymptotic limit, the change in entropy tends to zero in late time which shows that the entropy is extremized and thus the end phase is in an equilibrium state. As $q \rightarrow -1$ in the

future, the total entropy S becomes equal to the horizon entropy S_H , given by

$$S_{\text{future}} = \frac{8\pi^2}{H_0^2 \tilde{\Omega}_\Lambda} \quad (92)$$

The change in entropy, $\dot{S} \rightarrow 0$ implies that the total entropy stabilizes at the value S_{future} and does not increase any further, i.e. it reaches an asymptotic limit [119].

The evolution of \dot{S} with respect to redshift z is shown in Fig.17 using the best-fit values obtained for DS3. Figure shows the time derivative of entropy, \dot{S} remains positive throughout the cosmic evolution and tends towards zero in the future. Further, the equilibrium state may be stable or unstable according as $\ddot{S} < 0$ or $\ddot{S} > 0$ at least in the far future. We plot the evolution of \ddot{S} with respect to redshift which is shown in Fig.18. It is observed that $\ddot{S} > 0$ in the early phase of evolution and made a transition to $\ddot{S} < 0$ in the recent past. Thus, a thermodynamic stable equilibrium state is achieved in late time. As $z \rightarrow -1$, $\ddot{S} \rightarrow 0$ which shows that any system satisfying the extremum of entropy and convexity condition behaves like an ordinary macroscopic system. Therefore, we can say that the evolution of the Universe is like the evolution of an ordinary macroscopic system.

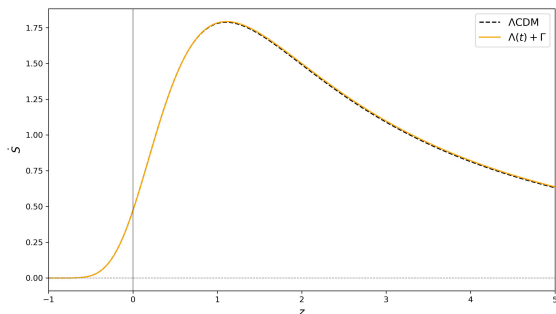


FIG. 17. Rate of change of entropy with respect to time from the best-fit values obtained for DS3. The positive value ensures that the entropy always increases. The dashed line shows the evolution for the standard model.

IX. CONCLUSION

In this work, we have studied the Universe's expansion powered by gravitationally induced 'adiabatic' matter creation and decaying vacuum in a spatially flat homogeneous and isotropic FLRW spacetime. We have demonstrated how matter creation affects the expanding Universe with a decaying vacuum, especially the late time evolution. As matter creation and varying $\Lambda(t)$ are phenomenological and have various forms in the literature, we have considered the specific forms for the vacuum energy density and matter creation rate, viz., $\rho_\Lambda = c_0 + 3\nu H^2$ and $\Gamma = 3\beta H$. Based on

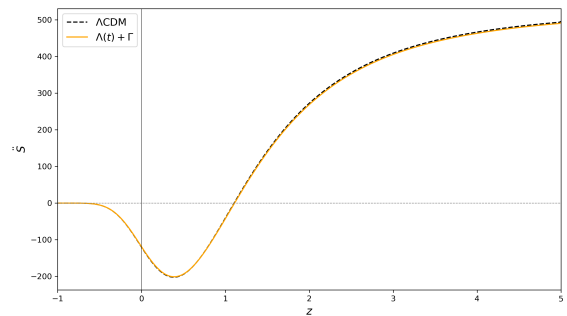


FIG. 18. Second derivative of entropy with respect to time from the best-fit values obtained from DS3 showing how the entropy accelerates with time. The dashed line shows the evolution for the standard model.

the latest observational data, the motivation was to study the dynamics of a cosmological model that has an interplay between the vacuum (dark energy) and the matter sector. The dynamical analysis confirms that the Universe's expansion is going through a cosmic acceleration phase. We have described this phenomenon using analytic solutions and observational constraints of the Hubble function and deceleration parameter. Our model's parameter constraints, which we obtained through the MCMC sampler, largely agreed with the Λ CDM model. We now present a summary of the key findings.

We have found the analytic solutions of the various cosmological parameters like $H(z)$, $q(z)$, $w_{\text{eff}}(z)$ and z_{tr} and then tested them with the latest observational data. Our results show that the Universe is currently in an accelerated expansion phase, having previously been in a decelerating phase. The transition redshift $z_{\text{tr}} = 0.675 \pm 0.019$ for DS1, $z_{\text{tr}} = 0.675 \pm 0.019$ for DS2 and $z_{\text{tr}} = 0.677 \pm 0.019$ for DS3 are consistent with Λ CDM and other recent constraints reported in the literature. The values for the effective EoS parameter for the three datasets were less than $-1/3$, which affirm the accelerating phase. Thus, the parameter constraints we obtained align with our understanding of DE in the Universe.

One thing we note is that our model favors strongly favors a value close to 0.700 ± 0.007 for the current value of the fractional density parameter Ω_Λ which is slightly higher than the values reported for the standard model and the Planck estimate 0.6889 ± 0.0056 . The tension between the two is around 1.24σ which is not significant. The residual tensions for the Hubble parameter constraints for our model in respect of the latest measurement of $H_0 = 73.04 \pm 1.04$ km/s/Mpc [114] for the three chosen datasets DS1, DS2, and DS3 are 4.07σ , 4.06σ , and 4.03σ respectively. We have explored cosmic perturbations and structure formation through the σ_8 and S_8 parameters, which were constrained through DS3 (Table II). The evolution of $f\sigma_8$ has been shown in

Figure 14, where theoretical curves of the weighted linear growth rate function for the Λ CDM and the $\Lambda(t) + \Gamma$ model have been plotted against the 18 $f(z)\sigma_8(z)$ data points. The curves are in agreement and consistent with the observational data. Our results align with the weak gravitational lensing observations [120] for both the standard model and the proposed model. However, there is some discrepancy between the best-fit values and the values obtained from the Planck 2018 results [121]: $\sigma_8 = 0.8102 \pm 0.0060$ and $S_8 = 0.825 \pm 0.011$.

We have also observed the evolution of the jerk parameter for our model (Figure 13), and for all three datasets, the parameter is positive and less than unity at early times. It tends towards unity in the future, mimicking the behaviour of the standard model, for which the parameter is always equal to one. The reduced χ^2 values for all three data combinations have also been calculated, and the values come out to be less than one, implying the model fits the observational data well and vice-versa. These values have been displayed in Table III. We have also used AIC and BIC selection criteria to discriminate between our chosen and the reference model, Λ CDM. According to the values of ΔAIC obtained for all three datasets, our model fits the data reasonably well, and there is averagely strong evidence in favour of it compared to the reference model. However, as per the ΔBIC values, the evidence is stacked against our model and is probably not a very good fit.

Following that, we have discussed a thermodynamic analysis for a Universe in our proposed scenario of matter creation and decaying vacuum. We found expressions for the dark matter temperature and the particle number density. We have discussed the GSL of thermodynamics for the proposed model. We have observed that the proposed model satisfies the GSL and convexity condition for the stability. We have shown these evolutions through the graphs of the first

derivative of entropy \dot{S} and its acceleration \ddot{S} in Figs. 17 and 18, respectively.

In conclusion, the phenomenological model depicting the interaction between dark matter with matter creation and decaying vacuum dark energy, as explored in the paper, effectively describes the evolutionary features of the Universe at both background and perturbation levels. The thermodynamic features are also in accordance with established laws. Thus, exploring the interaction between dark matter empowered by matter creation and decaying vacuum stems from diverse perspectives, and holds promise for future study. This involves employing dynamical system analysis to explore deeper insights into the evolution of the Universe.

CRedit authorship contribution statement

Lokesh Chander: Formal analysis, software, writing-original draft and **C P Singh:** Conceptualization, Methodology, Writing, review & editing.

Declaration of Competing interest

The authors declare that they have no known competing financial interests that could have appeared to influence the work reported in this paper.

Data availability

There are no new data associated with this research.

ACKNOWLEDGMENTS

One of the authors, L.C. would like to thank University Grant commission (UGC), India for granting Junior Research Fellowship to carry out this work.

-
- [1] A. G. Riess, et al., Observational evidence from supernovae for an accelerating universe and a cosmological constant, *Astron. J.* **116**, 1009 (1998).
 - [2] S. Perlmutter, et al., Measurements of Ω and Λ from 42 high-redshift supernovae, *Astrophys. J.* **517**, 565 (1999).
 - [3] D. J. Eisenstein, et al., Detection of the baryon acoustic peak in the large-scale correlation function of SDSS luminous red galaxies, *Astrophys. J.* **633**, 560 (2005).
 - [4] O. Farooq and B. Ratra, Hubble parameter measurement constraints on the cosmological deceleration-acceleration transition redshift, *Astrophys. J. Lett.* **766**, L7 (2013).
 - [5] D. Larson, et al., Seven-year wilkinson microwave anisotropy probe (WMAP*) observations: power spectra and WMAP-derived parameters, *Astrophys. J. Suppl.* **192**, 16 (2011).
 - [6] V. Sahni, Dark matter and dark energy, *Lect. Notes Phys.* **653**, 141 (2004). arXiv:astro-ph/0403324
 - [7] C. ORaifeartaigh, et al., One hundred years of the cosmological constant: from superfluous stunt to dark energy, *Eur. Phys. J. H* **43**, 73 (2018).
 - [8] V. Sahni and A. Starobinsky, The case for a positive cosmological Λ -term, *Int. J. Mod. Phys. D* **9**, 373 (2000).
 - [9] L. M. Krauss and M. S. Turner, The cosmological constant is back, *Gen. Relativ. Gravit.* **27**, 1137 (1995).
 - [10] S. M. Carroll, The cosmological constant, *Living Rev. Relativ.* **4**, 1 (2001).
 - [11] R. Schützhold, On the cosmological constant and the cosmic coincidence problem, *Int. J. Mod. Phys. A* **17**, 4359 (2002).
 - [12] S. Weinberg, The cosmological constant problem, *Rev. Mod. Phys.* **61**, 1 (1989).
 - [13] H. E. S. Velten, R. F. vom Marttens and W. Zimdahl, Aspects of the cosmological coincidence problem, *Eur. Phys. J. C* **74** 1 (2014).
 - [14] O. Bertolami, Time-dependent cosmological term, *Il*

- Nuovo Cimento B **93**, 36 (1986).
- [15] K. Freese, F. C. Adams, J. A. Frieman and E. Mottola, Cosmology with decaying vacuum energy, Nucl. Phys. B **287**, 797 (1987).
 - [16] J. A. S. Lima and M. Trodden, Decaying vacuum energy and deflationary cosmology in open and closed universes, Phys. Rev. D **53**, 4280 (1996).
 - [17] J. M. Overduin and F. I. Cooperstock, Evolution of the scale factor with a variable cosmological term, Phys. Rev. D **58**, 043506 (1998).
 - [18] I. L. Shapiro and J. Solà, Scaling behavior of the cosmological constant and the possible existence of new forces and new light degrees of freedom, Phys. Lett. B **475**, 236 (2000).
 - [19] I. L. Shapiro and J. Solà, The scaling evolution of the cosmological constant, J. High Energy Phys. **02**, 006 (2002).
 - [20] J. S. Alcaniz and J. M. F. Maia, Current and future supernova constraints on decaying Λ cosmologies, Phys. Rev. D **67**, 043502 (2003).
 - [21] R. Opher and A. Pelinson, Studying the decay of the vacuum energy with the observed density fluctuation spectrum, Phys. Rev. D **70**, 063529 (2004).
 - [22] F. Bauer, The running of the cosmological and the newton constants controlled by the cosmological event horizon, Class. Quant. Grav. **22**, 3533 (2005).
 - [23] S. Carneiro and J. A. S. Lima, Time -dependent cosmological term and holography, Int. J. Mod. Phys. A **20**, 2465 (2005).
 - [24] J. S. Alcaniz, J. A. S. Lima, Interpreting cosmological vacuum decay, Phys. Rev. D **72**, 063516 (2005).
 - [25] J. Solà and H. Štefančić, Effective equation of state for dark energy: Mimicking quintessence and phantom energy through a variable Λ , Phys. Lett. B **624**, 147 (2005).
 - [26] J. D. Barrow and T. Clifton, Cosmologies with energy exchange, Phys. Rev. D **73**, 103520 (2006).
 - [27] A. E. Montenegro Jr and S. Carneiro, Exact solutions of Brans–Dicke cosmology with decaying vacuum density, Class. Quant. Grav. **24**, 313 (2006).
 - [28] S. Basilakos, Cosmological implications and structure formation from a time varying vacuum, Mon. Not. R. Astron. Soc. **395**, 2347 (2009).
 - [29] I. L. Shapiro and J. Solà, On the possible running of the cosmological constant, Phys. Lett. B **682**, 105 (2009).
 - [30] M. Tong and H. Noh, Observational constraints on decaying vacuum dark energy model, Eur. Phys. J. C **71**, 1 (2011).
 - [31] J. Solà, Cosmologies with a time dependent vacuum, J. Phys.: Conf. Ser. **283**, (2011) 012033.
 - [32] J. A. S. Lima, S. Basilakos and J. Solà, Expansion history with decaying vacuum: a complete cosmological scenario, Mon. Not. R. Astron. Soc. **431**, 923 (2013).
 - [33] M. Szydlowski, A. Stachowski and K. Urbanowski, Cosmology with a decaying vacuum energy parametrization derived from quantum mechanics, J. Phys.: Conf. Ser. **626**, 012033 (2015).
 - [34] J. A. S. Lima, E. L. D. Perico and G. J. M. Zilotti, Decaying vacuum inflationary cosmologies: Searching for a complete scenario including curvature effects, Int. J. Mod. Phys. D **24**, 1541006 (2015).
 - [35] G. J. M. Zilotti, R. C. Santos and J. A. S. Lima, From de Sitter to de Sitter: Decaying vacuum models as a possible solution to the main cosmological problems, Adv. High Energy Phys. **2018** 6980486 (2018).
 - [36] C. P. Singh and J. S. Peracaula, Friedmann cosmology with decaying vacuum density in Brans-Dicke theory, Eur. Phys. J. C **81**, 1 (2021).
 - [37] C. P. Singh and V. Khatri, Viscous fluid dynamics with decaying vacuum energy density, Phys. Rev. D **109**, 023508 (2024).
 - [38] J. Solà, Dark energy: a quantum fossil from the inflationary universe?, J. Phys. A: Math. Theor. **41**, 164066 (2008).
 - [39] E. Schrödinger, The proper vibrations of the expanding universe, Physica **6**, 899 (1939).
 - [40] L. Parker, Particle creation in expanding universes, Phys. Rev. Lett. **21**, 562 (1968).
 - [41] L. Parker, Quantized fields and particle creation in expanding universes. I, Phys. Rev. **183**, 1057 (1969).
 - [42] I. Prigogine and J. Geheniau, Entropy, matter, and cosmology, Proc. Natl. Acad. Sci. U.S.A. **83**, 6245 (1986).
 - [43] I. Prigogine, et al., Thermodynamics of cosmological-matter creation, Proc. Natl. Acad. Sci. U.S.A. **85**, 7428 (1988).
 - [44] I. Prigogine, Thermodynamics and cosmology, Int. J. Theor. Phys. **28**, 927 (1989).
 - [45] M. O. Calvão, J. A. S. Lima and I. Waga, On the thermodynamics of matter creation in cosmology, Phys. Lett. A **162**, 223 (1992).
 - [46] J. A. S. Lima and A. S. M. Germano, On the equivalence of bulk viscosity and matter creation, Phys. Lett. A **170**, 373 (1992).
 - [47] J. A. S. Lima, A. S. M. Germano and L. R.W. Abramo, FRW-type cosmologies with adiabatic matter creation, Phys. Rev. D **53**, 4287 (1996).
 - [48] W. Zimdahl, J. Triginer and D. Pavón, Collisional equilibrium, particle production, and the inflationary universe, Phys. Rev. D **54**, 6101 (1996).
 - [49] V. Johri and K. Desikan, An extended class of FRW models with creation of particles out of gravitational energy, Astrophys. Lett. Commun. **33**, 287 (1996).
 - [50] J. S. Alcaniz and J. A. S. Lima, Closed and open FRW cosmologies with matter creation: kinematic tests, Astron. Astrophys. **349**, 729 (1999).
 - [51] W. Zimdahl, D. J. Schwarz, A. B. Balakin and D. Pavón, Cosmic antifriction and accelerated expansion, Phys. Rev. D **64**, 063501 (2001).
 - [52] Y. Qiang, T.-J. Zhang and Z.-L. Yi, Constraint on cosmological model with matter creation using complementary astronomical observations, Astrophys. Space Sci. **311**, 407 (2007).
 - [53] G. Steigman, R. C. Santos and J. A. S. Lima, An accelerating cosmology without dark energy, J. Cosmol. Astropart. Phys. **09**, 033 (2009).
 - [54] C. P. Singh and A. Beesham, Early universe cosmology with particle creation: kinematics tests, Astrophys. Space Sci. **336**, 469 (2011).
 - [55] C. P. Singh, FRW models with particle creation in Brans-Dicke theory, Astrophys. Space Sci. **338**, 411 (2012).
 - [56] J. A. S. Lima, S. Basilakos and F. E. M. Costa, New cosmic accelerating scenario without dark energy, Phys. Rev. D **86**, 103534 (2012).
 - [57] J. A. S. Lima, L. L. Graef, D. Pavón and S. Basilakos, Cosmic acceleration without dark energy: Background tests and thermodynamic analysis, J. Cosmol. Astropart. Phys. **14**, 042 (2014).

- [58] R. O. Ramos, M. V. dos Santos and I. Waga, Matter creation and cosmic acceleration, *Phys. Rev. D* **89**, 083524 (2014).
- [59] S. Pan, B. K. Pal and S. Pramanik, Gravitationally influenced particle creation models and late-time cosmic acceleration, *Int. J. Geom. Methods Mod. Phys.* **15**, 1850042 (2018).
- [60] C. P. Singh and A. Kumar, Quintessence behavior via matter creation cosmology, *Eur. Phys. J. C* **80**, 106 (2020).
- [61] Y. Bhardwaj and C. P. Singh, Matter creation cosmology with generalized Chaplygin gas, *Astrophys. Space Sci.* **369**, 2 (2024).
- [62] Z.-K. Guo and Y.-Z. Zhang, Cosmology with a variable Chaplygin gas, *Phys. Lett. B* **645**, 326 (2007).
- [63] J. Zheng, et al., Revisiting chaplygin gas cosmologies with the recent observations of high-redshift quasars, *Eur. Phys. J. C* **82**, 582 (2022).
- [64] F. Salahedin, R. Pazhouhesh and M. Malekjani, Cosmological constraints on new generalized Chaplygin gas model, *Eur. Phys. J. Plus* **135**, 429 (2020).
- [65] L. P. Chimento, et al., Interacting quintessence solution to the coincidence problem, *Phys. Rev. D* **67**, 083513 (2003).
- [66] L. Amendola, G. C. Campos and R. Rosenfeld, Consequences of dark matter-dark energy interaction on cosmological parameters derived from type Ia supernova data, *Phys. Rev. D* **75**, 083506 (2007).
- [67] R. Chowdhury and P. Rudra, Interacting generalized cosmic chaplygin gas in loop quantum cosmology: A singularity free universe, *Int. J. Theor. Phys.* **52**, 489 (2013).
- [68] H. Zhang, H. Yu, Z.-H. Zhu and Y. Gong, A quantitative criteria for the coincidence problem, *Phys. Lett. B* **678**, 331 (2009).
- [69] M. Özer and M.O. Taha, A model of universe free of cosmological problems, *Nucl. Phys. B* **287**, 776 (1987).
- [70] M. Gasperini, A thermal interpretation of the cosmological constant, *Class. Quantum Gravity* **5**, 521 (1988).
- [71] J. C. Carvalho, J. A. S. Lima and I. Waga, Cosmological consequences of a time-dependent Λ term, *Phys. Rev. D* **46**, 2404 (1992).
- [72] S. L. Adler, Einstein gravity as a symmetry breaking effect in quantum field theory, *Rev. Mod. Phys.* **54**, 729 (1982).
- [73] L. Parker and D. J. Toms, Explicit curvature dependence of coupling constants, *Phys. Rev. D* **31**, 2424 (1985).
- [74] S. Basilakos, M. Plionis and J. Solà, Hubble expansion and structure formation in time varying vacuum models, *Phys. Rev. D* **80**, 083511 (2009).
- [75] J. Solà, Cosmological constant and vacuum energy: old and new ideas, *J. Phys.: Conf. Ser.* **453**, (2013) 012015.
- [76] F. Andrade-Oliveira, F. E. M. Costa and J. A. S. Lima, Decaying vacuum cosmology and its scalar field description, *Class. Quantum Grav.* **31**, 045004 (2014).
- [77] J. Grande, J. Solà, S. Basilakos and M. Plionis, Hubble expansion and structure formation in the “running FLRW model” of the cosmic evolution, *J. Cosmol. Astropart. Phys.* **11** 007 (2011).
- [78] D. Bessada and O. D. Miranda, Probing a cosmological model with a $\Lambda = \Lambda_0 + 3\beta H^2$ decaying vacuum, *Phys. Rev. D* **88**, 083530 (2013).
- [79] A. P. Jayadevan, et al., Probing the dynamical system and thermal behaviors of the model, $\Lambda_0 + 3\beta H^2$, *Astrophys. Space Sci.* **364**, 1 (2019).
- [80] M. A. van der Westhuizen and A. Abebe, Interacting dark energy: clarifying the cosmological implications and viability conditions, *J. Cosmol. Astropart. Phys.* **2024**, 048 (2024).
- [81] R. Brandenberger, R. Kahn and W. H. Press, Cosmological perturbations in the early universe, *Phys. Rev. D* **28**, 1809 (1983).
- [82] V. F. Mukhanov, H. A. Feldman and R. H. Brandenberger, Theory of cosmological perturbations, *Phys. Rep.* **215**, 203 (1992).
- [83] K. A. Malik and D. Wands, Cosmological perturbations, *Phys. Rep.* **475** 1 (2009).
- [84] J. Solà Peracaula, J. de Cruz Pérez and A. Gómez-Valent, Possible signals of vacuum dynamics in the universe, *Mon. Not. R. Astron. Soc.* **478**, 4357 (2018).
- [85] J. de Cruz Pérez and J. S. Peracaula, Running vacuum in Brans - Dicke theory: A possible cure for the σ_8 and H_0 tensions, *Phys. Dark Universe* **43**, 101406 (2024).
- [86] W. J. C. da Silva and R. Silva, Growth of matter perturbations in the extended viscous dark energy models, *Eur. Phys. J. C* **81**, 403 (2021).
- [87] P. J. E. Peebles, *Principles of Physical Cosmology*, Princeton University Press, 1993.
- [88] Y.-S. Song and W. J. Percival, Reconstructing the history of structure formation using redshift distortions, *J. Cosmol. Astropart. Phys.* **09**, 004 (2009).
- [89] D. Huterer, et al., Growth of cosmic structure: Probing dark energy beyond expansion, *Astropart. Phys.* **63**, 23 (2015).
- [90] S. Nesseris and L. Perivolaropoulos, Testing Λ CDM with the growth function $\delta(a)$: Current constraints, *Phys. Rev. D* **77**, 023504 (2008).
- [91] B. Leibundgut, Type Ia supernovae, *Astron. Astrophys. Rev.* **10**, 179 (2000).
- [92] A. G. Riess, et al., Type Ia supernova discoveries at $z > 1$ from the hubble space telescope: Evidence for past deceleration and constraints on dark energy evolution, *Astrophys. J.* **607**, 665 (2004).
- [93] W. M. Wood-Vasey, et al., Observational constraints on the nature of dark energy: first cosmological results from the essence supernova survey, *Astrophys. J.* **666**, 694 (2007).
- [94] A. Conley, et al., Supernova constraints and systematic uncertainties from the first three years of the supernova legacy survey, *Astrophys. J. Suppl.* **192**, 1 (2010).
- [95] N. Suzuki, et al., The Hubble space telescope cluster supernova survey V improving the dark-energy constraints above $z > 1$ and building an early-typehosted supernova sample, *Astrophys. J.* **746**, 85 (2012).
- [96] M. Betoule, et al., Improved cosmological constraints from a joint analysis of the SDSS-II and SNLS supernova samples, *Astron. Astrophys.* **568**, 1 (2014).
- [97] D. H. Weinberg, et al., Observational probes of cosmic acceleration, *Phys. Rep.* **530**, 87 (2013).
- [98] D. J. Eisenstein, Dark energy and cosmic sound, *New Astron. Rev.* **49**, 360 (2005).
- [99] B. Bassett and R. Hlozek, Baryon acoustic oscillations, *Dark Energy: Observational and Theoretical Approaches*, Cambridge University Press, pp. 246 - 278 (2010), DOI: <https://doi.org/10.1017/CBO9781139193627.010>.

- [100] A. G. Adame, et al., Desi 2024 III: Baryon acoustic oscillations from galaxies and quasars, arXiv preprint (2024), doi:10.48550/arXiv.2404.03000.
- [101] A. G. Adame, et al., Desi 2024 VI: Cosmological constraints from the measurements of baryon acoustic oscillations, arXiv preprint (2024), doi:10.48550/arXiv.2404.03002.
- [102] E. Gawiser and J. Silk, The cosmic microwave background radiation, *Phys. Rep.* **333**, 245 (2000).
- [103] D. J. Fixsen, The temperature of the cosmic microwave background, *Astrophys. J.* **707**, 916 (2009).
- [104] D. J. Fixsen, et al., The cosmic microwave background spectrum from the full COBE FIRAS data set, *Astrophys. J.* **473**, 576 (1996).
- [105] Y. Wang and P. Mukherjee, Observational constraints on dark energy and cosmic curvature, *Phys. Rev. D* **76**, 103533 (2007).
- [106] Y. Wang and S. Wang, Distance priors from Planck and dark energy constraints from current data, *Phys. Rev. D* **88**, 043522 (2013).
- [107] M. Tristram *et al.*, Cosmological parameters derived from the final Planck data release (PR4), *Astron. Astrophys.* **682**, A37 (2024).
- [108] G. Liu, Y. Wang and W. Zhao, Testing the consistency of early and late cosmological parameters with BAO and CMB data, *Phys. Lett. B* **854**, 138717 (2024).
- [109] M. Moresco, et al., Unveiling the universe with emerging cosmological probes, *Living Rev. Relativ.* **25**, 6 (2022).
- [110] S. Nesseris, G. Pantazis and L. Perivolaropoulos, Tension and constraints on modified gravity parametrizations of $G_{eff}(z)$ from growth rate and planck data, *Phys. Rev. D* **96**, 023542 (2017).
- [111] D. Foreman-Mackey, et al., emcee: the MCMC hammer, *Publ. Astron. Soc. Pac.* **125**, 306 (2013).
- [112] R. Trotta, Bayes in the sky: Bayesian inference and model selection in cosmology, *Contemp. Phys.* **49**, 71 (2008).
- [113] N. Aghanim, et al., Planck 2018 results-VI. cosmological parameters, *Astron. Astrophys.* **641**, A6 (2020).
- [114] A. G. Riess, et al., A comprehensive measurement of the local value of the hubble constant with $1 \text{ km s}^{-1} \text{ Mpc}^{-1}$ uncertainty from the Hubble space telescope and the SH0ES team, *Astrophys. J. Lett.* **934**, L7 (2022).
- [115] H. Akaike, A new look at the statistical identification, *IEEE transactions on automatic control.* **19**, 716 (1974).
- [116] G. Schwarz, Estimating the dimension of a model, *Ann. Stat.* **6**, 461 (1978).
- [117] J.D. Bekenstein, Black holes and entropy, *Phys. Rev. D* **7**, 2333 (1973).
- [118] G. Izquierdo and D. Pavón, *Phys. Lett. B* **639**, 1 (2006).
- [119] S. Frautschi, Entropy in an expanding universe, *Science* **217**, 593–599 (1982).
- [120] C. Heymans, et al., KiDS-1000 Cosmology: Multi-probe weak gravitational lensing and spectroscopic galaxy clustering constraints, *Astron. Astrophys.* **646**, A140 (2021).
- [121] N. Aghanim *et al.*, Planck 2018 results—I. Overview and the cosmological legacy of Planck, *Astron. Astrophys.* **641**, A1 (2020).